Sulphide Segregation in Ferropicrites from the Pechenga Complex, Kola Peninsula, Russia

Article *in* Journal of Petrology · December 2000

DOI: 10.1093/petrology/41.12.1721 · Source: OAI

4 authors, including:

Gerhard Brügmann
Curt Engelhorn Zentrum Archäometrie
113 PUBLICATIONS **2,952** CITATIONS

SEE PROFILE

Eero Hanski
University of Oulu
148 PUBLICATIONS **2,572** CITATIONS

SEE PROFILE

JOURNAL OF PETROLOGY | VOLUME 41 | NUMBER 12 | PAGES 1721–1742 | 2000

Sulphide Segregation in Ferropicrites from the Pechenga Complex, Kola Peninsula, Russia

G. E. BRÜGMANN[1]*, E. J. HANSKI[2], A. J. NALDRETT[3] AND V. F. SMOLKIN[4]

[1]MAX-PLANCK-INSTITUT FÜR CHEMIE, ABT. GEOCHEMIE, POSTFACH 3060, 55020 MAINZ, GERMANY

[2]GEOLOGICAL SURVEY OF FINLAND, PO BOX 77, FIN-96101 ROVANIEMI, FINLAND

[3]DEPARTMENT OF GEOLOGY, UNIVERSITY OF TORONTO, TORONTO, ONT. M5S 3B1, CANADA

[4]GEOLOGICAL INSTITUTE, ACADEMY OF SCIENCES, SU-184200 APATITY, RUSSIA

RECEIVED MAY 18, 1999; REVISED TYPESCRIPT ACCEPTED APRIL 26, 2000

The Palaeoproterozoic Ni–Cu sulphide deposits of the Pechenga Complex, Kola Peninsula, occur in the lower parts of ferropicritic intrusions emplaced into the phyllitic and tuffaceous sedimentary unit of the Pilgujärvi Zone. The intrusive rocks are comagmatic with extrusive ferropicrites of the overlying volcanic formation. Massive lavas and chilled margins from layered flows and intrusions contain <3–7 ng/g Pd and Pt and <0·02–2·0 ng/g Ir, Os and Ru with low Pd/Ir ratios of 5–11. The abundances of platinum group elements (PGE) correlate with each other and with chalcophile elements such as Cu and Ni, and indicate a compatible behaviour during crystallization of the parental magma. Compared with the PGE-depleted central zones of differentiated flows (spinifex and clinopyroxene cumulate zones) the olivine cumulate zones at the base contain elevated PGE abundances up to 10 ng/g Pd and Pt. A similar pattern is displayed in intrusive bodies, such as the Kammikivi sill and the Pilgujärvi intrusion. The olivine cumulates at the base of these bodies contain massive and disseminated Ni–Cu-sulphides with up to 2 μg/g Pd and Pt, but the PGE concentrations in the overlying clinopyroxenites and gabbroic rocks are in many cases below the detection limits. The metal distribution observed in samples closely representing liquid compositions suggests that the parental magma became sulphide saturated during the emplacement and depleted in chalcophile and siderophile metals as a result of fractional segregation of sulphide liquids. Relative sulphide liquid–silicate melt partition coefficients decrease in the order of Ir > Rh > Os > Ru > Pt = Pd > Cu. R-factors (silicate-sulphide mass ratio) are high and of the order of 10^4–10^5, and they indicate the segregation of only small amounts of sulphide liquid in the parental ferropicritic magma. In differentiated flows and intrusions the sulphide liquids segregated and accumulated at the base of these bodies, but because of a low silicate–sulphide mass ratio the sulphide liquids had a low PGE tenor and Pt/Ir and Cu/Ir ratios similar to the parental silicate melts. During cooling the sulphide liquid crystallized 40–50% of monosulphide solid solution (mss) and the residual sulphide liquid became enriched in Cu, Pt and Pd and depleted in Ir, Os and Ru. The Cu-rich sulphide liquid locally assimilated components of the surrounding S-rich sediments as suggested by the radiogenic Os isotopic composition of some sulphide ores (γ_{Os} >100). Most of the massive and breccia ores represent mixtures of mss and residual Cu-rich sulphide liquid whereas chalcopyrite-rich veins formed when the Cu-rich sulphide liquids were squeezed out into the surrounding sediments.

KEY WORDS: *ferropicrite; Pechenga; magmatic Ni–Cu sulphide deposits; platinum-group elements*

INTRODUCTION

The Pechenga Complex belongs to the Russian part of the Kola Peninsula (Fig. 1). The Kola Peninsula represents the eastern part of the Fennoscandian (Baltic) Shield, which forms the Archaean basement of the Siberian Platform. The shield consists of Archaean granite–

*Corresponding author. E-mail: bruegman@mpch-mainz.mpg.de

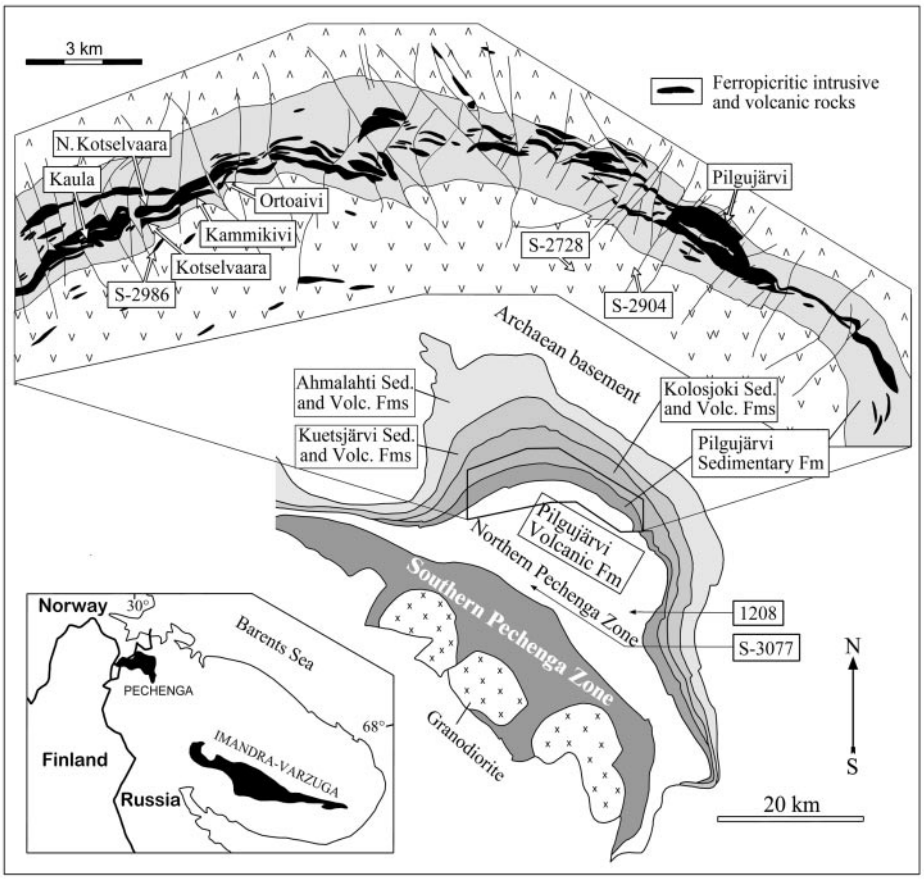

Fig. 1. Geological map of the Pechenga area and sample localities.

gneiss terrains and experienced several magmatic, metamorphic and tectonic episodes that lasted until the Caledonian–Hercynian magmatic events at 450–350 Ma.

The Kola Peninsula has six areas with Cu–Ni mineralization. Some of them occur in the Archaean basement, such as the Allarechka, East Pechenga and Lovnoozero areas (Papunen & Gorbunov, 1985). However, most deposits are associated with the Pechenga–Varzuga Zone, which is composed of Palaeoproterozoic volcanic–sedimentary rocks. The Pechenga Complex contains the most important Ni mineralization, and, of the deposits within the boundaries of the former USSR, is second only to the Ni-camp of Noril'sk in Siberia. The history of the discovery and mining activities has been described by Gorbunov *et al.* (1985*a*, 1985*b*) and Hanski (1992).

Data for Cu, Ni and the platinum group elements (PGE) from the Pechenga silicate and sulphide rocks are very scanty in the literature. Statistical parameters, such as variation coefficients, correlations and ratios of the Ni and Cu distribution in various ore deposits are published, but with the exception of the data of Abzalov & Both (1997), absolute concentrations for single deposits are not given or coded (Zak *et al.*, 1982; Distler *et al.*, 1990). Therefore, this study focuses on the discussion of the distribution of chalcophile and siderophile metals in typical gabbro–wehrlite intrusions and on the petrogenesis of sulphide ores from various Ni deposits in the Pechenga Complex. These data are complemented by a quantitative description of the chemical behaviour of these metals in ferropicritic lava flows.

Geology of the Pechenga Complex

The geology of the Pechenga Complex has been described in numerous publications (e.g. Gorbunov *et al.*, 1985*a*; Hanski & Smolkin, 1989, 1995; Hanski, 1992; Melezhik *et al.*, 1994*a*, 1994*b*; Smolkin, 1997; Melezhik & Sturt, 1998*a*, 1998*b*; Sharkov & Smolkin, 1998). In the following, only salient features are summarized and augmented with recent isotopic data to constrain the age relationships.

The Pechenga Complex belongs to the Archaean domain of the Fennoscandian Shield, which contains several large volcanic–sedimentary belts, such as the Onega

Plateau, the Imandra Zone or the Pechenga Complex. Puchtel *et al.* (1998) suggested that the upper parts of these belts are part of the same large igneous province. This formed during a single igneous event at ~2 Ga, when the Archaean basement was flooded and intruded by plume-derived mafic and ultramafic magmas. Thus, the Palaeoproterozoic Imandra Varzuga–Pechenga belt (Fig. 1) probably once formed a continuous sedimentary–volcanic basin, but is now faulted into two separate blocks. The Pechenga Complex has been divided into two structurally different parts, the Northern Pechenga Zone and the Southern Pechenga Zone (Fig. 1). Geological information about the Southern Pechenga Zone remains limited because of its poor exposure and highly deformed nature. As a result, its stratigraphic relation to the Northern Pechenga Zone is not well known, but recent isotopic studies have indicated a younger age of the Southern Pechenga Zone (Balashov, 1996; Smolkin *et al.*, 1996). The ferropicritic lava flows and intrusion studied here belong to the Northern Pechenga Zone, which is well preserved and well exposed.

The Northern Pechenga Zone forms a SE–SW-dipping (30–60°), asymmetric synclinorium with a length of 70 km and a maximum width of 30 km (Fig. 1). Remarkable features of the sequence are its great thickness (>8 km), long-lasting volcanism for almost 400 my, and the cyclic repetition of volcanic and sedimentary rocks. The rocks have undergone metamorphism varying from prehnite–pumpellyite or greenschist facies in the central part of the structure to amphibolite facies towards the peripheral zones. The Northern Pechenga Zone is divided into four major and conformable sedimentary–volcanic cycles, each of which commences with metasediments and ends with a much thicker pile of metavolcanic rocks. In the Russian literature, these cycles have been known as the Ahmalahti, Kuetsjärvi, Kolosjoki and Pilgujärvi suites (Zagorodnyi *et al.*, 1964). Melezhik *et al.* (1995) tried to adjust this nomenclature to the international recommendations for formal lithostratigraphical classification, giving each volcanic and sedimentary part of the suites formation status (for example, the Pilgujärvi Volcanic Formation) and assigning them to the North Pechenga Group. At the same time, Smolkin *et al.* (1995, 1996) presented a different formation- and group-level nomenclature. This among other disagreements on the geology of the Pechenga area generated a lively debate (Melezhik & Sturt 1998*a*, 1998*b*; Sharkov & Smolkin, 1998; Smolkin, 1998).

The ferropicrites and ore deposits occur in the youngest cycle, the Pilgujärvi suite. It begins with a thick sedimentary unit [the Pilgujärvi Sedimentary Formation after Melezhik *et al.* (1995); the Zdanov and Lammas Formations after Smolkin *et al.* (1995)], which forms an arc-like zone, extending with a northwesterly trend for >60 km and reaching its maximum thickness of ~1 km in the central part of the Pechenga structure (Fig. 1). The unit is made up of sandstones, siltstones, phyllites, and basaltic and picritic tuffs and tuffites. The fine-grained sediments are often enriched in carbonaceous matter and sulphides. The sedimentary unit is traditionally called 'the productive pile' (e.g. Gorbunov, 1968), for all the economic sulphide-bearing intrusions are located within this tuffaceous–sedimentary pile. In addition to nickeliferous gabbro–wehrlite intrusions, there are sill-like gabbro–diabase intrusions, which appear to be older than the gabbro–wehrlites (Gorbunov, 1968; Smolkin, 1977).

The uppermost and thickest volcanic unit of the Northern Pechenga Zone (the Pilgujärvi Volcanic Formation) is predominantly composed of tholeiitic basalts, which occur as hyaloclastites and pillow lavas. Volcanic rocks belonging to the ferropicritic rock suite make up ~4·5% of the total volume. The age of the ferropicrites is well constrained. Utilizing the Sm–Nd and Pb–Pb methods, Hanski *et al.* (1990) obtained whole-rock–mineral isochron ages of 1977 ± 55 and 1988 ± 39 Ma, respectively, for ferropicritic volcanic rocks and gabbro–wehrlite intrusions. Mitrofanov *et al.* (1991) obtained an Rb–Sr whole-rock isochron age of 1980 ± 44 Ma for tholeiitic volcanic rocks of the Pilgujärvi Volcanic Formation.

Petrography and geochemistry of the ferropicritic rock suite

Mineralogical compositions, major and trace element analyses and isotope studies of ferropicritic pillow lavas and tuffs, most magnesian spinifex-textured rocks, chilled margins of intrusions and layered flows and their weighted average compositions all attest that they formed from a common parental magma (Hanski & Smolkin, 1989, 1995; Sharkov & Smolkin, 1989; Skuf'in & Fedotov, 1989). Ferropicrites are mafic–ultramafic rocks and their MgO content often reaches 25 wt %. However, samples that represent liquid compositions do not exceed 19 wt % MgO (Hanski, 1992). Hanski & Smolkin (1989) emphasized the exceptionally high FeO content of the ultramafic lavas—they have an abundance maximum at 15–16 wt % of FeO_{tot} compared with a maximum at 11 wt % for most other primitive or primary magmas (Hanski, 1992). They defined these rocks as ferropicrites to distinguish them from komatiites. Ferropicrites have high TiO_2 and low Al_2O_3 contents resulting in a low Al_2O_3/TiO_2 ratio of about 3–4 (Hanski, 1992). This ratio is a fingerprint of olivine cumulates formed by ferropicritic magmas and can be used to distinguish them from olivine cumulates derived from komatiitic liquids. The ferropicrites are enriched in highly incompatible trace elements and display strongly fractionated rare earth element patterns with average La_N/Yb_N ratios of ~10

(Hanski, 1992). These features are typical of alkali basalts, but are not seen in komatiitic rocks, which commonly possess light rare earth element concentrations <10 times chondritic. Studies of radiogenic isotopes demonstrated that ferropicrites and gabbro–wehrlite intrusions were coeval and were derived from similar sources (Hanski *et al.*, 1990; Walker *et al.*, 1997). The unusual composition of the ferropicrite volcanic rocks implies that the parental magmas were formed in an Fe-rich and incompatible-element-rich source (Hanski & Smolkin, 1995). Even tholeiites from the Kolasjoki and Pilgujärvi Group appear to be Fe rich compared with Phanerozoic volcanic rocks (Hanski, 1992). Ferropicritic rocks have also been found in the Imandra–Varzuga belt, which attests to the presence of a large, compositionally distinct mantle reservoir beneath the Fennoscandian Shield at 2·0 Ga.

Ferropicritic lava flows

The ferropicritic rock suite comprises volcanic and intrusive gabbro–wehrlite bodies. The volcanic members occur as massive flows, pillow lavas, tuffs and layered, differentiated flows up to 50 m thick. Differentiated flows often display well-developed spinifex textures and a vertical zonation similar to those observed in differentiated komatiitic flows (Smolkin *et al.*, 1987; Hanski & Smolkin, 1989, 1991). The uppermost part of the flows consists of a chilled margin, the spinifex zone, and a zone with fine-grained, acicular pyroxenes and globules. Both olivine and clinopyroxene spinifex rocks occur in the upper part of the flows. The lower part of the flows consist of olivine(–chromite) cumulates overlain by thin pyroxene cumulates.

Ferropicritic intrusions

The ferropicrite magma also formed gabbro–wehrlite intrusions, which, in general, occur conformably with respect to the primary bedding of the enclosing sedimentary rocks (Zak *et al.*, 1982). Along strike they can be followed from 100 m to several kilometres, and although the largest one, the Pilgujärvi intrusion, attains a thickness of 470 m (Smolkin, 1977; Fig. 2), about half of the intrusions are <20 m thick (Zak *et al.*, 1982).

The magmatic cumulates underwent metamorphic and metasomatic alterations to varying degrees, leading ultimately to the formation of serpentinites, soapstone, etc. Nevertheless, the original textures are frequently preserved and the primary cumulus and intercumulus minerals can generally be recognized. A geological map of the Pilgujärvi layered intrusion, and a profile of it and the Kammikivi sill are shown in Figs 2–4. The differentiated intrusions are composed of an olivine cumulate at the bottom passing upwards through a generally thin clinopyroxenite to a gabbroic upper part. Quartz gabbro or potassium-feldspar-bearing essexite represent the last differentiates in the largest intrusions. The crystallization sequence of the cumulus minerals is generally chrome spinel, olivine, clinopyroxene, titanomagnetite and plagioclase. In the Pilgujärvi intrusion olivine and titanomagnetite occurred simultaneously as liquidus phases and produced olivine–magnetite cumulates in the middle part of the body (Fig. 2). Orthopyroxene is typically absent in all ferropicritic rocks. Primary hydrous minerals, kaersutite and titanian phlogopite–biotite occur as intercumulus minerals throughout the intrusions. In the following, the petrographic and chemical variations observed in the Pilgujärvi intrusion and Kammikivi sill will be described in more detail, because they show features typical for many intrusions of the Pechenga Complex and are the subject of this study.

Pilgujärvi intrusion. In the Pilgujärvi intrusion, Smolkin (1977) distinguished seven zones based on the texture and the cumulate and interstitial mineralogy of the rocks. Zones 1 and 7 represent the upper and lower chilled margins of the intrusion (Figs 2 and 3). They are very heterogeneous and consist of fragments of country rock, injections of quartz diorite and pyroxenites, which often contain variable amounts of plagioclase or olivine. The ultramafic part near the base of the intrusion (zone 2) has the highest *mg*-number of 0·72–0·75 (MgO 27–35 wt %; Table 1), whereas the concentrations of Al_2O_3 (2·2–5·2 wt %) and incompatible elements, such as P_2O_5 (0·04–0·15 wt %; Table 1), are low. Variable proportions of cumulus minerals such as olivine, chromite and sulphides, and interstitial phases such as clinopyroxene, amphibole, plagioclase and ilmenite can explain the composition of these samples. The composition and mineralogy of the intermediate zone (zone 3) indicate a transitional character between the ultramafic and mafic parts of the intrusion. At the base it consists of pyroxenites and olivine pyroxenites, which are overlain by rocks defined by Smolkin (1977) as kazanskite (titanomagnetite-rich pyroxene–olivine cumulates or wehrlites with FeO_{tot} >30 wt %) and kosvite (titanomagnetite-rich olivine pyroxenite with FeO_{tot} >20 wt %). The top of this intermediate horizon comprises plagiopyroxenite, which is rich in titanomagnetite. The next zone, zone 4, contains gabbros with pyroxenite interlayers, and the overlying zones 5 and 6 consist of gabbro cumulates with variable textures (Figs 2 and 3). From base to top the MgO contents systematically decrease (Table 1), whereas Al_2O_3 and P_2O_5 increase to 14 and 0·25 wt % (Table 1), respectively, in the upper gabbroic part.

Kammikivi sill. The Kammikivi sill comprises a chilled gabbro with devitrified glass at the top overlying a clinopyroxene cumulate (Fig. 4). The sill is mainly composed of olivine(–chromite) cumulates with sulphide mineralization at the bottom. The sulphide-poor olivine cumulates in the Kammikivi sill (at depths 24–40 m in Table 2) have *mg*-number of 0·66–0·75. The *mg*-number

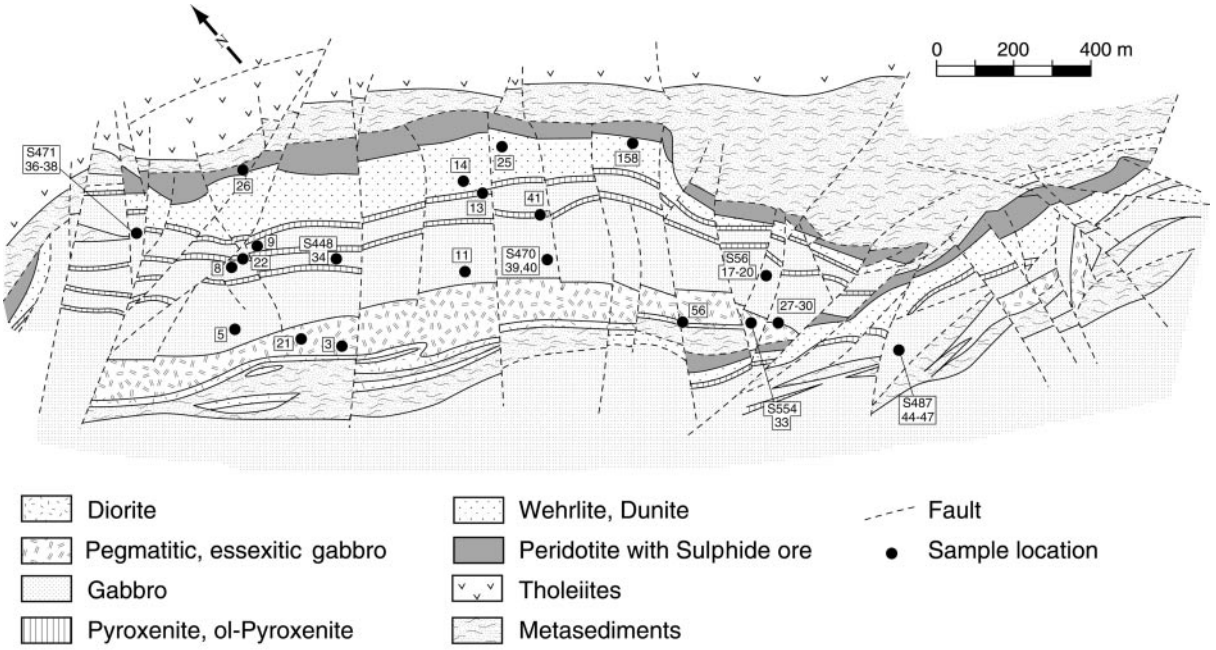

Fig. 2. Geological map of the Pilgujärvi intrusion in the eastern central part of the productive pile (Fig. 1) and sample locations [modified from Smolkin (1977)].

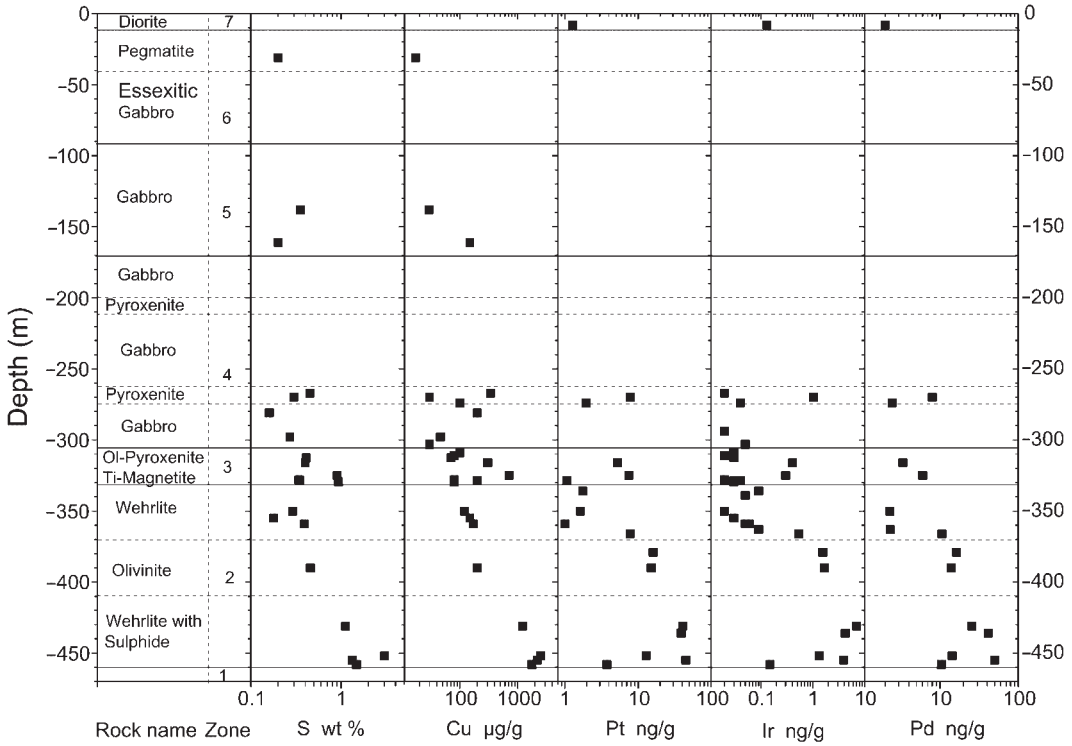

Fig. 3. Variation of S, Cu, Pt, Ir and Pd along a stratigraphic profile of the Pilgujärvi intrusion. Sulphur and metal concentrations systematically increase towards the base of the intrusion, which can be explained by accumulation of sulphides in the lower part of the intrusion.

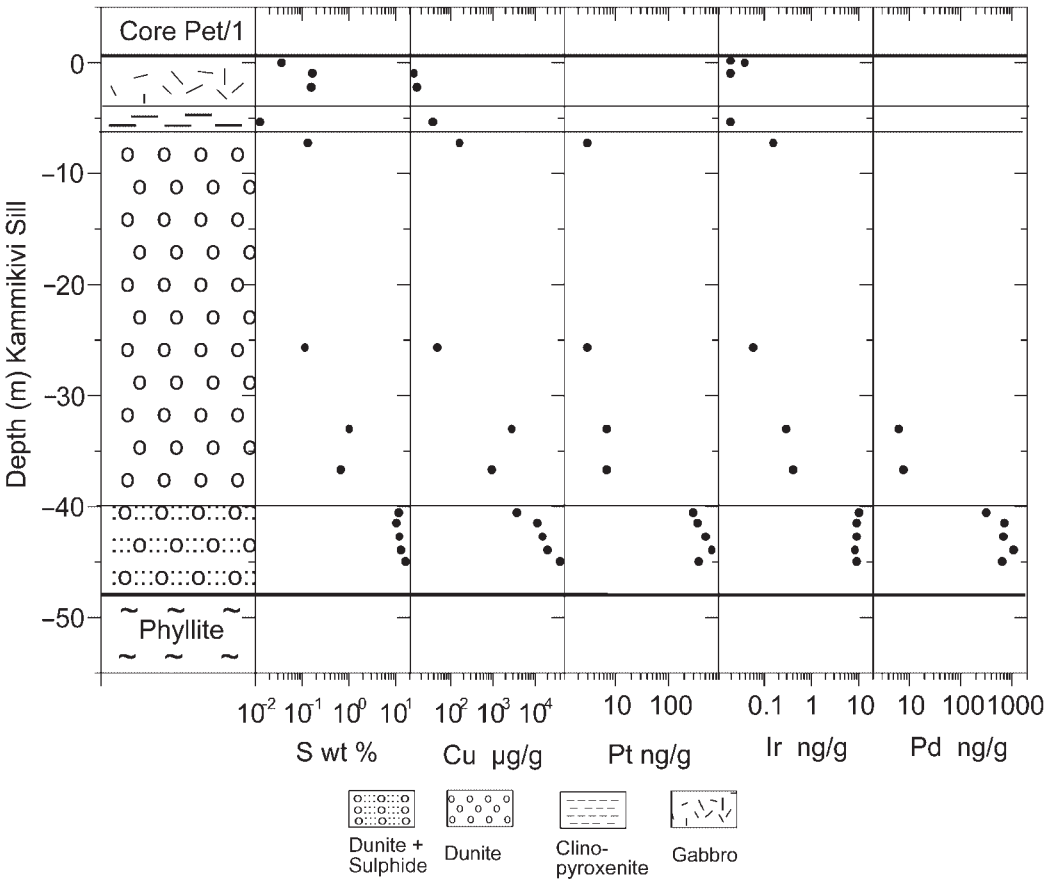

Fig. 4. Variation of S, Cu, Pt, Ir and Pd along a stratigraphic profile of the Kammikivi Sill. The highest concentrations are found at the base of the ultramafic cumulates. The correlation of S with Cu and PGE concentrations suggests that the amount of sulphide controls the distribution of these elements in the sill.

systematically decreases upward through the pyroxenite into the gabbroic zone, which has *mg*-numbers between 0·36 and 0·40. Oxide concentrations such as Al_2O_3 or P_2O_5 increase from the dunites towards the gabbro at the top of the sill from <5 to 15, and from <0·1 to 0·4 wt %, respectively (Table 2; Hanski, 1992).

The Ni-sulphide deposits

According to Zak *et al.* (1982), 226 intrusions have been found in the ore field and 25 contain Ni–Cu deposits of economic interest. The major ore-bearing intrusions occur in the sedimentary part of the Pilgujärvi Formation and are concentrated in its central, thickest part (Gorbunov *et al.*, 1985*a*, 1985*b*; Fig. 1).

According to Gorbunov (1968), the Ni–Cu sulphide ores at Pechenga generally display the following asymmetric pattern. The lowermost part of a mineralized zone, at the tectonic contact of the country rock with a layered intrusion, consists of breccia and massive ores of variable thicknesses. This is overlain by a zone of disseminated ores, a few metres to 100 m thick. The contacts between disseminated and massive ore, as well as between barren and mineralized serpentinites, are usually gradual. Most of the sulphide ore bodies are associated with the ultramafic parts of differentiated intrusions. In some deposits sulphides are not confined to the intrusive parent bodies, but extend for some distance into the enclosing tuffaceous–sedimentary rocks as small veins and impregnations (Gorbunov, 1968).

Pyrrhotite, pentlandite and chalcopyrite are the main ore minerals in all ore types. The average proportions of sulphide minerals in the disseminated ore are pyrrhotite 45%, pentlandite 40% and chalcopyrite 15% (Distler *et al.*, 1990). Minor ore minerals include pyrite, magnetite, violarite, sphalerite, bornite, cubanite, mackinawite and valleriite. Distler *et al.* (1990) also described platinum group minerals of the cobaltite–gersdorffite series in several sulphide deposits.

Gorbunov *et al.* (1985*a*) reported that Ni concentrations range from 1 wt % in low-grade disseminated ore to 10–12 wt % in massive and breccia ore. Mineralized phyllites contain up to 2 wt % Ni. Gorbunov *et al.* (1985*a*)

Table 1: Trace element distribution in the cumulates and sulphide ores from the Pilgujärvi intrusion

Sample	Depth (m)	MgO (wt %)	*mg*-no.	Al_2O_3 (wt %)	P_2O_5 wt %	Cu (μg/g)	S (μg/g)	Ni (μg/g)	Rh (ng/g)	Pd (ng/g)	Au (ng/g)	Pt (ng/g)	Ir (ng/g)	Os (ng/g)	Ru (ng/g)
Sa-56	8	14·31	0·58	8·12	0·25	n.d.	n.d.	130	0·1	2	0·30	1	0·13	0·2	0·7
Sa-3	24	2·12	0·24	14·56	0·48	n.d.	n.d.	n.d.	<0·05	<2	0·15	<1	<0·02	<0·1	<0·5
Sa-21	31	3·88	0·34	13·24	0·43	17	2000	20	<0·06	<2	0·33	<1	<0·02	<0·1	<0·5
Sa-11	138	4·53	0·34	13·63	0·23	29	3557	12	<0·13	<4	0·10	<1	<0·02	<0·1	<0·5
Sa-5	161	5·29	0·38	13·32	0·15	150	2000	300	<0·1	n.d.	0·15	<1	<0·02	<0·1	<0·5
Sa-41	267	9·53	0·44	6·05	0·08	340	4500	300	<0·05	<2	0·39	<1	0·02	<0·1	<0·5
Sa-22	270	10·71	0·50	5·79	0·03	30	3000	60	0·5	8	5·88	8	1·04	1·3	4·6
Sa-158	274	12·60	0·61	8·78	0·17	100	n.d.	280	<0·1	2	2·54	2	0·04	<0·1	<0·5
Sa-8	281	7·28	0·45	13·93	0·07	200	1600	80	<0·06	<2	0·15	<1	<0·02	<0·1	<0·5
Sa-044	294	n.d.	n.d.	n.d.	n.d.	n.d.	n.d.	n.d.	<0·07	<2	0·40	<1	0·02	<0·1	<0·5
Sa-9	298	7·24	0·47	13·43	0·06	46	2696	21	<0·06	<2	0·15	<1	<0·02	<0·1	<0·5
Sa-19	303	5·94	0·41	14·04	0·09	30	n.d.	70	<0·1	n.d.	0·22	<1	0·05	0·1	<0·5
Sa-16	309	7·78	0·44	11·66	<0·01	100	n.d.	100	<0·06	<2	0·32	<1	0·03	<0·1	<0·5
Sa-20	311	7·49	0·42	11·44	0·12	80	n.d.	90	<0·07	<2	0·17	<1	0·02	<0·1	<0·5
Sa-15	313	10·01	0·42	5·87	0·05	70	4100	140	<0·06	<2	0·16	<1	0·03	<0·1	<0·5
Sa-367	316	28·61	0·75	4·51	0·11	300	4000	2100	0·3	3	1·29	5	0·41	1·0	<0·5
134-8	325	n.d.	n.d.	n.d.	n.d.	717	9050	1120	0·5	6	1·75	8	0·30	0·2	<0·5
Sa-34	328	17·73	0·75	2·97	0·06	80	3400	300	<0·06	<2	0·16	<1	<0·02	<0·1	<0·5
Sa-36	329	16·23	0·68	4·29	<0·01	200	3500	480	<0·06	<2	0·35	1	0·04	<0·1	<0·5
Sa-39	329	n.d.	n.d.	n.d.	n.d.	n.d.	n.d.	n.d.	<0·06	<2	0·94	<1	0·03	<0·1	<0·5
Sa-368	330	19·86	0·68	6·25	0·13	80	9400	1100	<0·06	<2	0·43	<1	0·03	0·1	<0·5
Sa-37	336	n.d.	n.d.	n.d.	n.d.	n.d.	n.d.	n.d.	<0·1	n.d.	0·45	2	0·09	0·1	<0·5
Sa-46	339	n.d.	n.d.	n.d.	n.d.	n.d.	n.d.	n.d.	<0·1	<4	0·23	<1	0·05	<0·1	<0·5
Sa-40	350	31·82	0·74	2·97	0·07	120	2900	1900	<0·1	2	0·35	2	0·02	<0·1	<0·5
Sa-369	355	27·55	0·71	4·49	0·10	150	1800	1000	<0·05	<2	0·19	<1	0·03	<0·1	<0·5
Sa-14	359	32·95	0·75	3·26	0·05	170	3900	1500	<0·05	<3	0·44	1	0·05	<0·1	<0·5
Sa-27	363	n.d.	n.d.	n.d.	n.d.	n.d.	n.d.	n.d.	<0·06	2	0·74	1	0·09	<0·1	<0·5
Sa-38	366	n.d.	n.d.	n.d.	n.d.	n.d.	n.d.	n.d.	0·6	11	1·55	8	0·54	1·0	1·2
Sa-28	379	n.d.	n.d.	n.d.	n.d.	n.d.	n.d.	n.d.	1·2	16	6·40	16	1·56	2·5	3·2
Sa-25	390	31·77	0·70	2·20	0·04	200	4600	1600	1·0	14	12·39	15	1·68	2·1	4·1
Sa-370	431	29·47	0·73	3·66	0·12	1227	11197	3532	2·9	26	50·02	41	6·98	9·2	9·7
Sa-33	436	n.d.	n.d.	n.d.	n.d.	n.d.	n.d.	n.d.	2·3	41	5·76	39	4·26	5·8	5·4
Sa-26b	455	27·12	0·72	5·21	0·15	2200	13300	5300	3·9	50	27·10	45	3·92	6·8	8·7
Sa-73	458	34·98	0·75	2·29	<0·01	1760	14800	5800	0·4	10	2·63	4	0·15	0·3	<0·5

n.d., not determined; *mg*-number based on FeO(tot).

Table 2: Trace element distribution in the differentiated Keskitunturi flow and Kammikivi sill

Rock type	Depth (m)	MgO (wt %)	*mg*-no.	Al_2O_3 (wt %)	P_2O_5 wt %	Cu (μg/g)	S (μg/g)	Ni (μg/g)	Rh (ng/g)	Pd (ng/g)	Au (ng/g)	Pt (ng/g)	Ir (ng/g)	Os (ng/g)	Ru (ng/g)
Differentiated Keskitunturi Flow, drill hole S-2986															
Spinifex	76	6·84	0·46	14·02	0·40	50	10700	23	<0·1	<4	1·81	<1	0·06	<0·1	<0·5
Spinifex	76·5	6·63	0·43	13·02	0·35	30	4360	56	0·1	<6	5·13	1	0·22	<0·1	<0·5
Cpx cumulate	81·5	7·59	0·49	10·99	0·26	270	360	92	0·6	<2	2·80	5	0·67	<0·1	<0·5
Cpx cumulate	83·6	18·19	0·74	5·91	0·17	n.d.	n.d.	n.d.	0·2	4	0·40	4	0·09	<0·1	<0·5
Cpx cumulate	84·1	18·80	0·74	6·43	0·17	260	310	298	0·2	<4	1·03	2	0·27	<0·1	<0·5
Ol cumulate	93·5	25·97	0·73	4·74	0·13	190	2830	1419	1·0	11	5·05	11	1·50	1·7	2·9
Ol cumulate	97·9	19·46	0·73	7·03	0·16	130	190	632	0·3	<5	5·77	5	0·63	0·4	2·0
Kammikivi Intrusion, drill hole Pet-1															
Differentiated liquid	0·05	5·68	0·36	11·61	0·40	n.d.	370	26	<0·1	<2	0·92	<1	0·04	<0·1	<0·5
Differentiated liquid	0·08	n.d.	n.d.	n.d.	n.d.	n.d.	n.d.	n.d.	<0·1	<2	0·64	<1	0·02	<0·1	<0·5
Differentiated liquid	1·00	5·38	0·38	12·57	0·37	14	1740	30	<0·1	<2	6·67	<1	0·02	<0·1	<0·5
Quench gabbro	2·25	7·25	0·40	11·57	0·34	16	1610	7	<0·1	<2	0·32	<1	<0·02	<0·1	<0·5
Pyx cumulate	5·40	16·27	0·69	5·52	0·17	40	130	75	<0·1	<2	0·63	<1	0·02	<0·1	<0·5
Pyx cumulate	7·30	17·85	0·73	4·73	0·11	167	1360	152	<0·1	<2	0·12	3	0·16	0·3	<0·5
Ol cumulate	25·70	29·60	0·74	3·67	0·13	50	1180	1769	<0·1	<2	0·82	3	0·06	<0·1	<0·5
Ol cumulate	33·10	31·80	0·75	3·78	0·11	2919	10440	5160	0·4	6	7·09	7	0·30	0·2	1·3
Ol cumulate	36·70	27·60	0·68	4·52	0·14	979	7000	3477	0·4	8	0·89	7	0·42	0·3	1·6
Ol + sulphide cumulate	40·60	22·15	0·45	1·84	0·06	3903	118550	31116	15·2	331	37·7	301	10·4	7·0	13·2
Ol + sulphide cumulate	41·50	24·12	0·48	1·52	0·05	11998	109440	37264	10·7	750	58·6	373	9·19	4·2	n.d.
Ol + sulphide cumulate	42·75	21·09	0·41	1·44	0·04	15544	123580	46578	16·9	699	58·9	525	9·20	5·6	n.d.
Ol + sulphide cumulate	44·00	19·57	0·38	1·33	0·04	20320	134620	50669	15·1	1116	162	678	8·54	4·6	5·5
Ol + sulphide cumulate	45·05	13·12	0·26	1·36	0·04	40920	164160	36932	15·8	659	50·3	380	9·24	5·5	n.d.

n.d., not determined; *mg*-number based on FeO(tot).

and Zak *et al.* (1982) emphasized the large Cu variation in each ore type. In massive and breccia ores, Cu contents range from <1 to 13 wt %. High-grade disseminated ore has, on average, 4–6 wt % Cu, and phyllite-hosted ores are dominated by chalcopyrite and contain up to 10 wt % Cu (Gorbunov *et al.*, 1985*a*).

SAMPLE DESCRIPTION AND ANALYTICAL METHODS

Sample location and description

Ninety-two samples representing massive and differentiated lava flows, sulphide-bearing intrusions and the different types of sulphide ore have been taken from outcrop and drill cores. Most drill-hole and outcrop locations are shown in Fig. 1, except the locations of the samples from the Pilgujärvi intrusion, which are indicated in Fig. 2. The samples from the massive and pillowed flows are from drill hole S-3077 and outcrops I-1963 and I-1968. The latter samples are ferropicrites from the Tominga suite, which is part of the Imandra–Varzuga Zone (Fig. 1, Table 3). These samples should provide information on the composition and evolution of the ferropicritic liquid. In addition, such information can be obtained from samples of chilled margins of intrusions [from the Kaula, Kotselvaara (Table 3) and Pilgujärvi intrusions (SA-56, Table 1)], and from samples of the spinifex zone of differentiated lava flows [samples from drill core S-2986 (76, 76·5 m) and 1208/2, 1208/3, S-3R/731·4 in Tables 2 and 3]. The chemical composition of samples taken along profiles of intrusions, such as the Pilgujärvi intrusion (Fig. 3) and Kammikivi sill (Fig. 4), and of differentiated lava flows from drill hole S-2986 (Table 2) and outcrop 1208 (Table 3) are used to investigate the evolution of the ferropicritic magma. Although most of these samples are cumulates, and thus do not represent liquid compositions, together with the samples from Ni–Cu-sulphide ore from the Pilgujärvi intrusion and Kammikivi and Ortoavi sills (Tables 2 and 4) their compositions monitor the history of sulphide saturation, the segregation of the sulphide liquid and the formation of the sulphide deposits.

Analytical methods

The data for PGE, MgO, Al_2O_3, P_2O_5, Cu and Ni of massive and differentiated lava flows and intrusions, and for sulphide ores, are given in Tables 1–4.

Major element and S, Cu and Ni analyses were performed by conventional X-ray fluorescence spectrometry (XRF) using Philips PW 1400 spectrometers at the research laboratory of the Rautaruukki Co. in Raahe, Finland, and at the Geological Survey of Finland in Espoo. Most of the major and lithophile trace element data have been previously published (Hanski, 1992). PGE and Au were determined using neutron activation analysis after preconcentrating the PGE and Au into a sulphide bead from samples of 20–40 g. Asif & Parry (1989, 1990) and Brügmann *et al.* (1993) have described the method. On the basis of 22 analyses of the PGE standard SARM-7, the latter workers reported standard deviations (SD) of <7%, except for Au, for which SD is 34%. The results of duplicate analyses reported in Tables 1–4 are generally within these errors. However, near the detection limits the error increases to as high as 50%. The detection limits (background plus 3 SD) are 2 ng/g for Pd, 1 ng/g for Pt, 0·1 ng/g for Rh and Os, 0·5 ng/g for Ru, and 0·04 ng/g and 0·02 ng/g for Au and Ir, respectively.

RESULTS: DISTRIBUTION OF SIDEROPHILE AND CHALCOPHILE ELEMENTS IN SILICATES AND SULPHIDES

Abundance of siderophile and chalcophile metals in lava flows

The samples from lava flows comprise cumulates and rocks closely reflecting liquid compositions of the ferropicritic magma. The latter samples (filled symbols in Fig. 5) contain 0·4–1·7 wt % S, 89–660 μg/g Cu and 136–1700 μg/g Ni (Table 3; Fig. 5a). The highest PGE concentrations have been found in massive flows and pillow lavas from drill hole 3077, which contain up to 7 ng/g Pt and Pd, 0·8 ng/g Os and Ir, 2 ng/g Ru and 0·6 ng/g Rh. However, consideration of all samples representing liquid compositions reveals that PGE concentrations vary by at least one order of magnitude, and many samples have PGE contents that are below the detection limit of the analytical technique. Gold concentrations also vary over a large range from 0·16 to 3·94 ng/g, but do not show good correlations with any of the elements discussed here. This is probably caused by mobilization during hydrothermal alteration or may be due to analytical uncertainties, and further discussion of its distribution will not be pursued.

Samples from the chilled margin, spinifex zone or the gabbroic upper parts of differentiated flows have PGE variations that are similar to those of the massive flows. Thus, the fine-grained gabbro from the Lammas flow has PGE concentrations approaching the maximum values observed in massive ferropicrites (Table 3), but concentrations in the spinifex zone of the differentiated flow recovered in drill hole S-2986 are not detectable (Table

Table 3: Trace element distribution in ferropicritic massive flows, pillow lavas, spinifex zones and the Lammas flow

Sample	Location	Rock type	Depth (m)	MgO (wt %)	*mg*-no.	Al_2O_3 (wt %)	P_2O_5 wt %	Cu (μg/g)	S (μg/g)	Ni (μg/g)	Rh (ng/g)	Pd (ng/g)	Au (ng/g)	Pt (ng/g)	Ir (ng/g)	Os (ng/g)	Ru (ng/g)
Picrites: massive and pillow lavas, spinifex zone																	
Sa-243	Kaula	Lower margin		19·58	0·69	10·43	0·28	220	2580	487	<0·1	2	0·31	1	0·05	<0·2	<0·5
Sa-244	Kaula	Lower margin		19·51	0·68	9·08	0·25	270	8890	815	<0·1	3	0·33	2	0·07	<0·2	<0·5
Sa-245	Kaula	Lower margin		20·40	0·67	7·17	0·21	660	17300	1700	0·4	7	3·94	4	0·48	0·7	<0·5
3R/731.4	Kaula	Spinifex		9·06	0·52	9·70	0·29	170	3760	136	0·2	<4	1·88	2	0·20	0·2	0·7
3077/314.3	Shulgjaur	Massive lava		16·03	0·65	8·09	0·22	170	620	941	0·5	<5	1·31	6	0·79	0·9	2·1
3077/322.5	Shulgjaur	Pillow lava		17·01	0·66	8·10	0·21	200	530	1046	0·6	7	1·19	6	0·80	0·8	2·0
3077/3	Shulgjaur	Pillow lava		n.d.	n.d.	n.d.	n.d.	n.d.	n.d.	n.d.	0·4	4	0·60	4	0·44	0·5	1·5
3077/4	Shulgjaur	Pillow lava		n.d.	n.d.	n.d.	n.d.	n.d.	n.d.	n.d.	0·3	3	0·19	4	0·34	0·5	<0·5
3077/5	Shulgjaur	Pillow lava		16·91	0·67	6·91	0·22	174	390	898	0·4	2	0·57	5	0·46	0·4	<0·5
I-1963	Imandra–Varzuga	Pillow lava		8·42	0·48	10·92	0·31	90	1940	251	<0·1	<2	0·72	3	0·15	<0·2	<0·5
I-1968	Imandra–Varzuga	Pillow lava		14·94	0·61	9·99	0·28	160	210	468	0·2	<4	1·22	5	0·32	0·2	<0·5
Ortoavi-42c	Ortoaivi	Massive lava		13·42	0·58	8·22	0·25	180	3310	605	0·1	3	1·02	3	0·26	0·5	0·8
2728a		Massive lava		n.d.	n.d.	n.d.	n.d.	n.d.	n.d.	n.d.	0·3	3	0·48	3	0·24	0·3	<0·5
Kotsel0.01/0.04	Northern Kotselvaara	Chilled margin		19·91	0·70	9·44	0·27	89	2150	541	<0·1	<2	0·16	1	0·05	<0·2	<0·5
Kotsel0.25	Northern Kotselvaara	Chilled margin		19·30	0·67	9·92	0·25	249	5070	833	<0·1	<2	0·17	2	0·04	<0·2	<0·5
Lammas Flow, differentiated																	
1208/2		Spinifex	4	15·79	0·62	7·73	0·30	190	250	320	0·3	6	1·30	4	0·45	0·3	1·4
1208/3		Spinifex	7	11·85	0·60	10·55	0·33	220	160	228	0·2	8	1·88	3	0·43	<0·1	1·0
1208/5		Pyx cumulate	20	18·93	0·75	6·15	0·17	260	80	230	0·2	<4	1·51	3	0·41	<0·1	<0·5
1208/6		Ol cumulate	30	20·95	0·67	6·45	0·22	360	4850	1450	0·2	3	0·49	8	0·16	<0·1	0·7
1208/7		Ol cumulate	38	26·07	0·76	4·72	0·15	120	1390	1560	0·3	3	0·63	4	0·27	0·5	<0·5
1208/8		Ol cumulate	42	31·99	0·79	4·25	0·14	60	1050	n.d.	0·4	<4	1·04	4	0·58	1·3	1·4
1208/9		Ol cumulate	45	22·77	0·73	5·03	0·16	110	3410	1340	<0·1	<2	0·94	2	0·19	0·6	<0·5
1208/10		Ol cumulate	49·5	20·41	0·69	9·55	0·26	90	170	626	0·2	<4	1·20	4	0·45	0·4	1·7

n.d., not determined; *mg*-number based on Fe(tot).

Table 4: S, Ni, Cu and PGE concentrations in sulphide ores from various deposits in the Pechenga Complex

Sample	Location	Ore type	Cu (μg/g)	S (μg/g)	Ni (μg/g)	Rh (ng/g)	Pd (ng/g)	Au (ng/g)	Pt (ng/g)	Ir (ng/g)	Os (ng/g)	Ru (ng/g)
26	Kaula	Massive	39900	260000	70700	30·8	308	96·7	151	24·3	53·7	79·0
26	Kaula	Massive	39900	260000	70700	29·4	300	94·1	145	22·1	48·4	72·1
28	Kaula	Massive	42800	172000	50000	23·7	272	210·0	243	16·6	16·1	48·1
28	Kaula	Massive	42800	172000	50000	20·8	263	221·0	222	17·2	17·9	
65	Pilgujärvi	Breccia	4970	143000	37700	16·7	57	20·0	55	16·4	21·7	24·3
116-2	Pilgujärvi	Pelite xenolith	474	135000	1460	3·1	17	1·5	15	1·0	1·6	
116-2	Pilgujärvi	Pelite xenolith	474	135000	1460	2·2	18	0·6	14	0·8	1·4	
236-1	Pilgujärvi	Breccia	8070	85000	38100	13·2	197	393·5	74	18·7	29·4	31·9
256-1	Pilgujärvi	Disseminated	1370	112000	22000	17·1	297	9·8	124	16·4	36·5	48·5
37/3	Pilgujärvi	Disseminated	21000	82000	39300	22·5	445	46·2	340	19·6	36·5	24·9
37/3	Pilgujärvi	Disseminated	21000	82000	39300	20·5	429	51·1	305	19·7	50·7	27·2
Kotsel-2	Kotselvaara	Disseminated	42100	143000	37700	14·2	1019	22·0	738	6·9	2·4	2·3
Kotsel-2	Kotselvaara	Disseminated	42100	143000	37700	14·7	900	29·0	696	5·8		
Kotsel-1	Kotselvaara	Disseminated	25100	104000	52800	12·0	560	9·5	417	8·6	4·3	3·2
Ortoaivi1	Ortoavi	Disseminated	20500	105000	55300	18·9	1175	34·0	1172	12·3	3·3	
Ortoaivi1	Ortoavi	Disseminated	20500	105000	55300	22·1	1321	28·0	1224	9·9	4·5	2·0
Ortoaivi2	Ortoavi	Disseminated	15300	163000	38000	11·9	277	109·0	200	5·0	4·6	
Ortoaivi2	Ortoavi	Disseminated	15300	163000	38000	13·1	455	90·0	375	6·1	3·4	
S-2904/5	Ortoavi	Massive	12300	324000	22700	18·2	1182	9·5	732	5·1	4·3	6·4

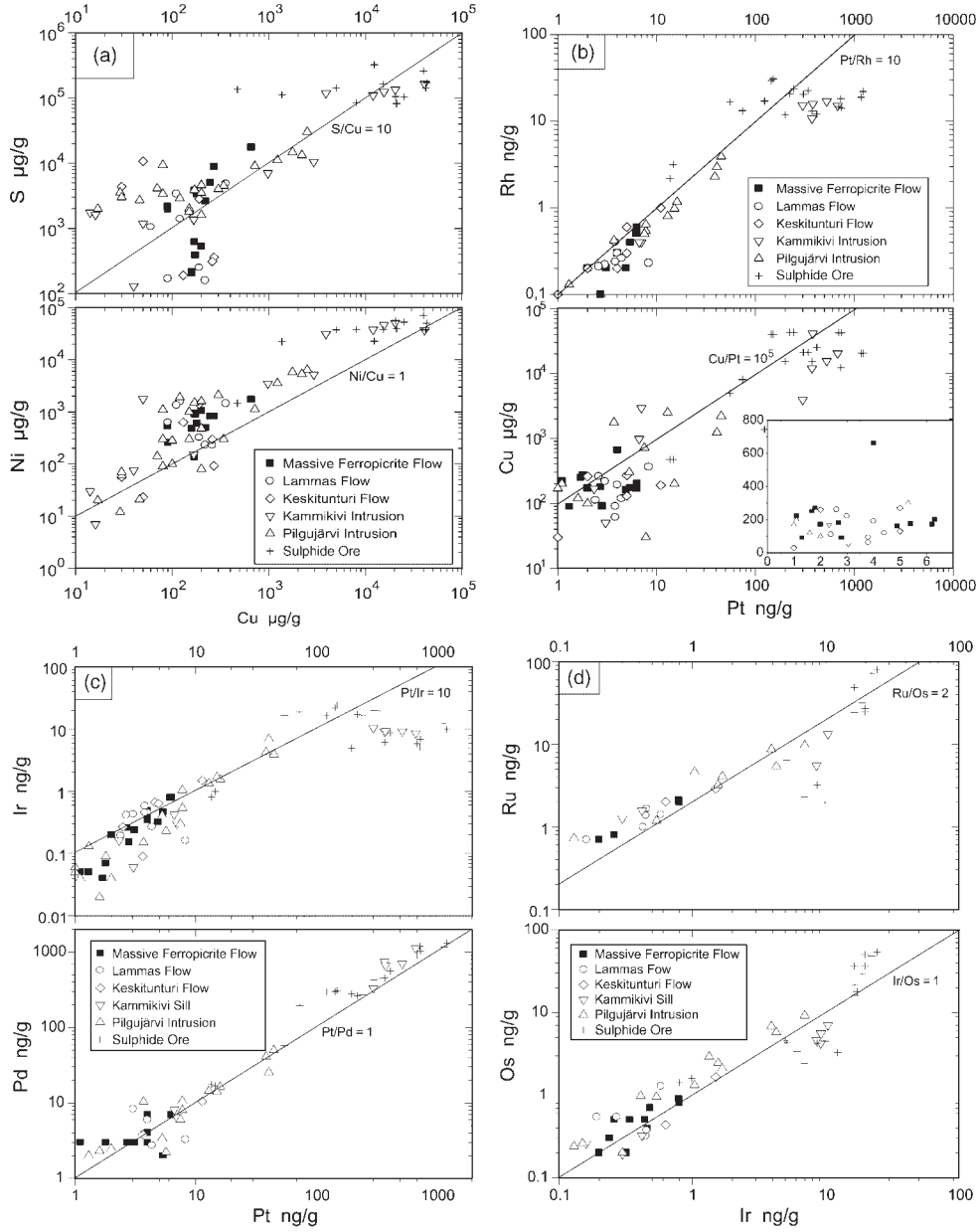

Fig. 5. Variation diagrams of S, Cu, Ni, and PGE. It should be noted that all elements are positively correlated regardless of the type of rock. This indicates that their distribution is controlled by accumulation and segregation of sulphide liquids. (a) Correlation of Cu with Ni and S. There are in general good correlations among these elements although they are partly obscured by secondary mobilization, especially of S and Cu. (b) Correlation of Pt with Cu and Rh. There is a broad positive correlation between Pt and Cu. Pt and Rh concentrations correlate well except at high Pt contents (>100 ppb), when Pt still increases but Rh remains rather constant. (c) Correlation of Pt with Pd and Ir. There is a good correlation between Pd and Pt indicating similar sulphide–silicate partition coefficients. The correlation between Pt and Ir is not well defined, mainly because at Pt concentrations of >100 ng/g, Ir concentrations stay rather constant. (d) Correlation of Ir with Os and Ru. With the exception of a few sulphide samples, there are very good correlations among these three elements. Although there is some scatter the Os/Ir ratio is close to chondritic value (1·3) whereas the Ru/Os ratio tends to be greater than the chondritic value (1·7).

2). There is no systematic PGE distribution along stratigraphic profiles of either of the differentiated flows (Tables 2 and 3) and the PGE variation in cumulates overlaps with that observed in the massive flows (Fig. 5b–d).

Abundance of siderophile and chalcophile metals in intrusions and sulphide ores

There is a continuum of PGE, Ni, Cu and S abundances as one proceeds from sulphide-poor or sulphide-free

cumulate rocks from flows to cumulate and massive sulphide samples from intrusions. The PGE, Ni, Cu and S concentrations in sulphur-poor cumulates from the Kammikivi and Pilgujärvi intrusions overlap with those found in the ferropicritic flows (Fig. 5). Samples from various deposits (Pilgujärvi, Kammikivi, Kotselvaara, Ortoaivi) containing disseminated sulphides and representing massive sulphides have 0·2–7·1 wt % Ni and 0·04–4·3 wt % Cu (Fig. 5a; Tables 2–4). Nickel and Cu show a good correlation despite a variable Ni/Cu ratio varying between one and 10 (Fig. 5a). These concentrations lie within the range published by Zak *et al.* (1982) and Gorbunov *et al.* (1985*a*). The concentrations of both elements increase with the S content (Fig. 5a). However, there is considerable scatter at any given S content. For example, in samples with similar S (10–20 wt %) and Ni contents (3–6 wt %) Cu concentrations vary by almost a factor of 100 from ~0·04 to 4 wt % (Fig. 5a).

The highest PGE concentrations have been found in massive sulphides containing up to 1·3 μg/g Pt and Pd, 31 ng/g Rh, 20 ng/g Ir, 50 ng/g Os and 80 ng/g Ru (Fig. 5b–d). The concentrations of all PGE show positive trends with the main components of the sulphides; for example, Pt with Cu in Fig. 5b. These features indicate that the abundances of chalcophile elements and precious metals are controlled by the amount of sulphide present in the rocks. This is also suggested by the PGE distribution in the silicate part of individual intrusions that are associated with sulphide deposits, such as the Kammikivi sill and the Pilgujärvi intrusion (Figs 3 and 4). These bodies have several features in common. The olivine-rich cumulates near the bottom of the igneous bodies have the highest concentrations of chalcophile elements and PGE. The concentrations of these elements also tend to increase gradually towards the lower margin. The gabbroic zones show decreasing Cu and PGE contents, commonly with PGE data below the detection limits. In both intrusions the S content increases towards their base, indicating that it is the accumulation of sulphide that governs the abundances of the PGE in the cumulates.

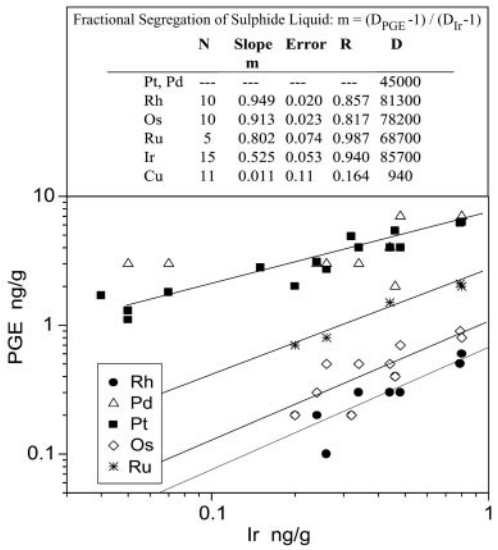

Fig. 6. Determination of sulphide liquid–silicate melt partition coefficients based on the assumption that the linear correlation between Ir and the other PGE are the result of fractional segregation of a sulphide liquid. The error of the slope (*m*) is represented by 1 SD.

DISCUSSION

PGE behaviour during the evolution of the ferropicritic magma

To understand the compositions of the sulphide ores and to constrain their formation, the abundances of chalcophile and siderophile elements in the parental ferropicritic liquid have to be estimated. The highest PGE concentrations observed in the ferropicritic massive flows approach those observed in other ultramafic magmas with 15–19 wt % MgO, such as komatiites (Brügmann *et al.*, 1987; Lesher, 1989). Many other samples representing liquid compositions, including spinifex-textured rocks and chilled margins, have significantly lower PGE contents. Normalized to a primitive mantle composition, the ferropicrites show distribution patterns typical for mantle-derived melts, where Pd, Pt and Cu are enriched relative to Ir, Os, Ru and Ni. They have Pd/Ir and Pt/Ir ratios ranging from two to 61; that is, values that are typical for ultramafic magmas. Although the mantle source of the magmas had an unusually high FeO content and enrichment of highly incompatible elements, the PGE contents in the ferropicrites provide no evidence for unusual absolute or relative PGE abundances in the mantle source.

The correlations of Cu and Ni with S are not well defined in massive flows, which is probably due to secondary mobilization of S. However, the Cu and Ni contents suggest a positive trend despite some scatter probably caused by postmagmatic disturbance of Cu. All PGE concentrations in the massive ferropicrite lavas indicate a positive correlation with each other (Figs 5 and 6). The coherent variation of Cu–Ni, Pt–Ir and Pd–Ir is surprising, because it is generally observed that Cu, Pd and Pt behave incompatibly and Ni and Ir compatibly in ultramafic magmas. Therefore, these element pairs should show a negative slope in variation diagrams such as those in Figs 5c and 6.

The coherent behaviour of the PGE during the crystallization of the ferropicritic magma is indicated in Fig. 7a, where the abundances of chalcophile and siderophile elements are normalized to the concentrations of the sample that has the highest PGE contents (sample 3077/

322·5; Table 3). The major element composition and the Cu and Ni contents of this sample lie within the range of the presumed parental magma compositions. All others show parallel distribution patterns relative to this sample. As the PGE concentrations decrease so do the Ni abundances. The decrease of the Ni content does not correlate with the MgO content because a few samples with high MgO content have low Ni contents (Kotsel 0·01, Kaula Sa-243; Table 3). Therefore, the variation of Ni in the ferropicritic flows cannot be explained by fractionation of olivine alone. In addition, it appears that Cu does not behave as an incompatible element such as, for example, P_2O_5. In the massive ferropicrite lavas, the P_2O_5 concentration increases from ~0·2 to 0·35 wt % as MgO decreases, as a result of the removal of olivine and some clinopyroxene (Fig. 8a). In contrast, Cu concentrations tend to decrease from ~250 to <100 μg/g (Fig. 8b). Combined these two observations results in a negative correlation between P_2O_5 and Cu. A similar variation would be observed between Pd, Pt and P_2O_5. The apparently compatible behaviour of Cu, Pd and Pt (and the same can be recognized for the other PGE) is best explained by the segregation of a sulphide liquid. This implies that most of the ferropicrite flows studied here were sulphide saturated at the time of their emplacement. The sulphur content of the ferropicrite flows is high, ranging from ~500 to 3000 μg/g (Table 3), although S is not a reliable monitor of sulphide saturation in the ferropicrite magma, because it does not exhibit systematic trends with MgO, P_2O_5 or Cu (Fig. 5a). Some samples of chilled margins and spinifex zones have unreasonably high S contents of up to 1·7% (Tables 2 and 3), which indicates postmagmatic S addition. Other samples, for example, Kaula Sa-245, also have unusually high Cu contents (Fig. 8b). As this sample has also high S and PGE concentrations (Table 3), this pattern probably reflects the accumulation of small amounts of sulphide. However, a secondary redistribution of Cu may also have contributed to this enrichment.

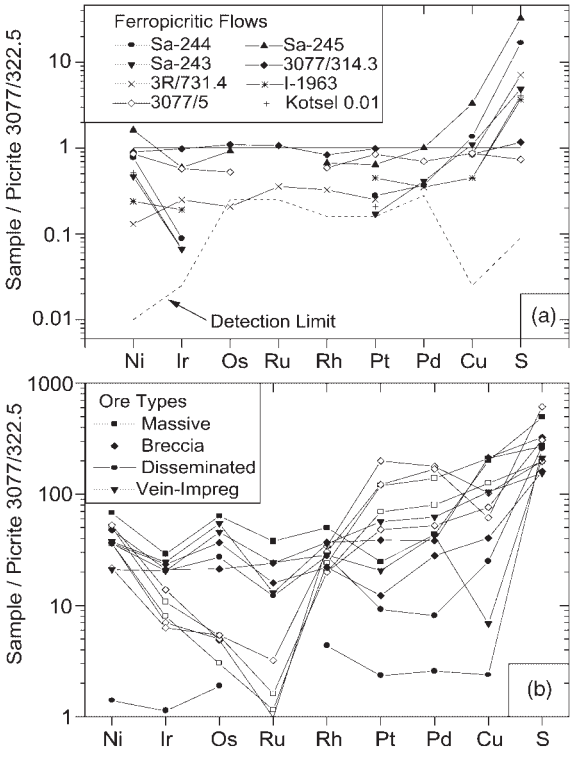

Fig. 7. Distribution patterns of the PGE, Cu, S and Ni in (a) ferropicritic flows and (b) different ore types. The concentrations of the samples have been normalized to the least PGE-depleted ferropicrite sample, which probably reflects the PGE abundances in the sulphur-undersaturated ferropicritic magma.

Determination of the sulphide liquid–silicate melt partition coefficients

Additional evidence for the segregation of a sulphide liquid is the observation that chalcophile and siderophile elements fractionate according to their sulphide liquid–silicate melt partition coefficients. Depending on the amount of sulphide fractionation, the silicate liquid should become less depleted in moderately chalcophile elements, such as S, Cu and Ni ($D_{sil/su}$ <1000), relative to highly chalcophile elements, such as the PGE ($D_{sil/sul}$ >10 000). The Cu–Pt variation (Fig. 5b) supports this presumption, because concentrations of the moderately chalcophile element Cu in the ferropicrites vary by less than a factor of two, whereas concentrations of the highly chalcophile metal Pt vary by a factor of six. Supporting evidence is also seen in Fig. 9, where the ratios of metals with different sulphide–silicate partition coefficients vary as a function of the concentration of Ir. As the Ir concentration decreases in the ferropicrites, that is, as a sulphide liquid segregates from the picritic magma, metal ratios such as Pt/Ir and Cu/Ir increase. The extent of this increase depends on the selected metal pair, and hence on the difference between their chalcophile affinities. For example, the Pt/Ir ratio increases from about eight to 48, whereas the Cu/Ir value increases by more than one order of magnitude from 0·2 to 7 (Fig. 9). These variations suggest that the sulphide–silicate partition coefficient increases in the order Cu < Pt < Ir, which is consistent with experimental data (Stone *et al.*, 1990; Bezmen *et al.*, 1994; Peach *et al.*, 1994).

The metal variation in the ferropicritic melt can be described quantitatively if one assumes that the fractionation of sulphide liquid and silicate–oxide minerals can be modelled by a non-equilibrium process such as fractional crystallization:

$$C_L = C_0 F^{(D-1)} \quad (1)$$

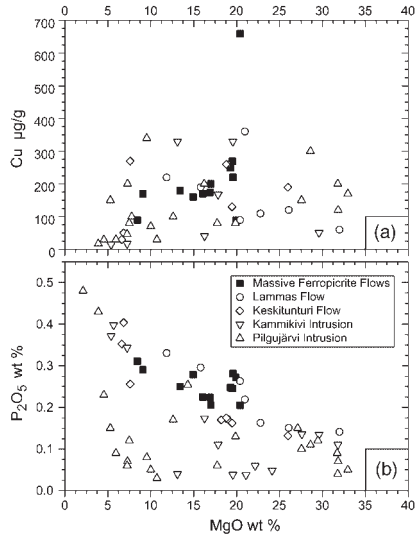

Fig. 8. Relationship of lithophile and chalcophile elements in S-poor samples from massive ferropicritic flows and cumulates of differentiated flows and intrusions. (a) MgO vs P_2O_5 concentrations. In the ferropicrite flows P_2O_5 behaves like an incompatible element, becoming more enriched as the liquids crystallizes. (b) In contrast, Cu behaves like a compatible element, as its concentration decreases with decreasing MgO content. This suggests that most of the picrite samples are S saturated.

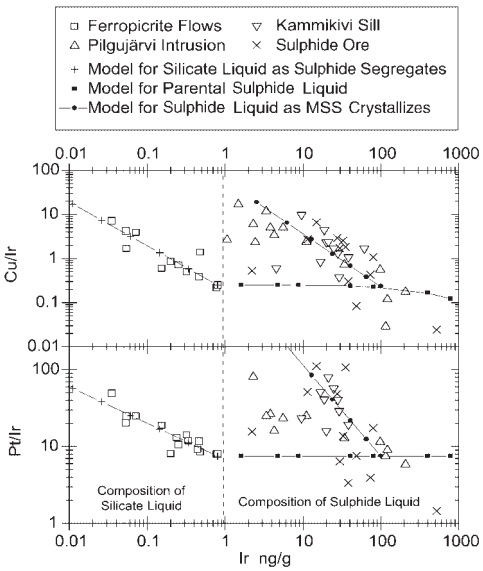

Fig. 9. Observed and predicted Pt/Ir and Cu/Ir ratios as a function of the Ir content in massive and differentiated ferropicritic flows, intrusions and sulphide ores. The Ir content of the sulphide samples has been recalculated to 100% sulphide. The trend defined by crosses represents the calculated evolution of the parental ferropicritic melt (P); 10^{-5}% of sulphide liquid segregate at each step. The trend defined by filled squares reflects the composition of a sulphide liquid in equilibrium with the parental ferropicritic melt as a function of the silicate–sulphide mass ratio (R = 1–1000). The trend defined by filled circles represents the calculated evolution of the parental sulphide liquid; 10% of monosulphide solid solution crystallizes at each step. (For details of the calculations see text and Table 5.)

where C_0 and C_L are the concentrations in the parental and residual liquids, respectively, F is the melt fraction and D represents the bulk partition coefficient. Given this case, two elements (A and B) should define a linear relationship in a log A vs log B diagram. The slope (m) of this line is a measure of the relative bulk partition coefficients (D_A, D_B) of the two elements, because it can be shown that

$$m = (D_A - 1)/D_B - 1). \quad (2)$$

Such a diagram is shown in Fig. 6, where the concentrations of Pt, Pd, Rh, Os and Ru are plotted against Ir. The slopes of the different element pairs indicate that the bulk partition coefficients decrease in the order Ir > Rh > Os > Ru > Pt = Pd > Cu. This succession reflects the sequence of sulphide–silicate liquid partition coefficients determined in experiments (Stone *et al.*, 1990; Bezmen *et al.*, 1994; Peach *et al.*, 1994) and suggests that the calculated relative bulk partition coefficients actually represent sulphide–silicate partition coefficients. The variation of the PGE concentrations in the lava flows is thus mainly determined by the segregation of a sulphide liquid and not significantly modified by the crystallization of silicate and oxide phases such as olivine or chromite. This can be demonstrated by calculating the relative partition coefficients for two extreme endmember models (Table 5). One model assumes that the metal variation can be explained by fractional segregation of pure sulphide liquid. In this case, the relative sulphide–silicate partition coefficient for Ir and Pt (D_{Ir}/D_{Pt}) is 1·904 (see Fig. 6 and Table 5). The second model assumes the joint fractionation of silicate–oxide minerals (99%) and sulphide liquid (1%). Given that Pd is incompatible (D^{Pt}_{silox} = 0·01) whereas Ir is compatible (D^{Ir}_{silox} = 10) in silicate and oxide phases, D_{Ir}/D_{Pt} is 1·927 (Table 5). Despite the different behaviour of Ir and Pt with regard to silicate–oxide phases, their crystallization together with a sulphide liquid would increase the relative partition coefficient of these elements by just 1·1%. Considering the uncertainties in the slope (10–20% for the PGE; Fig. 6), the calculated relative bulk partition coefficients indeed represent relative sulphide–silicate partition coefficients. To estimate the absolute partition coefficients for all the PGE, a value of 45 000 for Pd was used in Fig. 6 (Bezmen *et al.*, 1994; Peach *et al.*, 1994). The resulting estimates for the other metals lie within the range of experimentally determined partition coefficients (Stone *et al.*, 1990; Bezmen *et al.*, 1994; Peach *et al.*, 1994).

The sulphide–silicate partition coefficients estimated above provide an internally consistent database, which can be used to describe the observed PGE and Cu variation in the ferropicrite flows. Assuming fractional segregation and that the ferropicrite with the highest

Table 5: Models describing the PGE distribution in the ferropicrite melt and sulphide liquid

Parameters	Ir (ng/g)	Pt (ng/g)	Cu (μg/g)	Pt/Ir	Cu/Ir × 1000
C_{sil}^0	0·8	6	200	7·5	0·25
C_{sul}^0	100	750	23000	7·5	0·23
$D_{silox/sil}$	10	0·01	0·1		
$D_{sul/sil}$	85700	45000	940		
$D_{sul+silox}$	867	450	9·5		
$D_{mss/sul}$	5	0·25	0·2		

Models of fractional segregation of sulphide liquid

Model 1

Segregation of pure sulphide liquid

R1,2	F1	Ir (ng/g) C_{sil}^1	Pt/Ir C_{sil}^1	Cu/Ir × 1000 C_{sil}^1
	1	0·80	7·50	0·25
99999	0·99999	0·34	11·27	0·58
49999	0·99998	0·14	16·93	1·36
33332	0·99997	0·06	25·43	3·18
24999	0·99996	0·03	38·20	7·42
19999	0·9995	0·01	57·39	17·32

Model 2

Fractionation of silicate/oxide + sulphide

F2	Ir (ng/g) C_{sil}^2	Pt/Ir C_{sil}^2	Cu/Ir × 1000 C_{sil}^2
1	0·80	7·50	0·25
0·9990	0·34	11·38	0·59
0·9980	0·14	17·28	1·39
0·9970	0·06	26·24	3·29
0·9960	0·02	39·88	7·77
0·9950	0·01	60·62	18·38

Model concentration in sulphide liquid (C_{sul}^0)

R	Ir (ng/g)	Pt/Ir	Cu/Ir × 1000
1	1·6	7·50	0·25
5	4·8	7·50	0·25
10	8·8	7·50	0·25
50	40·8	7·50	0·24
100	80·7	7·49	0·23
500	398	7·46	0·16
1000	792	7·42	0·12

Model of sulphide crystallization (C_{sul}^1)

FS	Ir (ng/g)	Pt/Ir	Cu/Ir × 1000
1	100	7·5	0·2
0·9	65·6	12·4	0·4
0·8	41·0	21·6	0·7
0·7	24·0	40·8	1·3
0·6	13·0	84·9	2·7
0·5	6·3	202	6·4
0·4	2·6	582	18·7

C_{sil}^0, concentration in parental silicate magma; C_{sul}^0, concentration in parental sulphide magma; $D_{silox/sil}$, silicate/oxide–silicate liquid partition coefficient; $D_{sul/sil}$, sulphide–silicate liquid partition coefficient; $D_{sul+silox}$, bulk partition coefficient of Model 2: 99% silicate/oxide + 1% sulphide; $D_{mss/sul}$, monosulphide solid solution–sulphide liquid partition coefficient; F1, F2, fraction of residual silicate liquid in models 1 and 2; FS, fraction of residual sulphide liquid; R1,2, mass ratio silicate to sulphide liquid in models 1 and 2.

PGE concentration has suffered insignificant sulphide fractionation the model predicts an increase of ratios such as Pt/Ir and Cu/Ir, as variable amounts of sulphide liquid segregate (Fig. 9). The calculated fractionation trends agree well with the observed PGE variation in the ferropicrites in terms of absolute abundances and metal ratios. These calculations also indicate that only very small amounts of sulphide had to segregate, because the mass ratio of silicate to sulphide liquid is high, ranging from 10^4 to 10^5 (Table 5).

Petrogenesis of the sulphide ores

The first investigators of the Pechenga Complex, geologists of the Geological Commission of Finland, favoured the magmatic concept, in which sulphide liquids form by sulphide immiscibility in mafic and ultramafic magmas and settle to the base of the magma body (Väyrynen, 1938). This idea was based on the close association of the sulphide ores with the ultramafic part of intrusions, as well as on the chemical composition of the sulphides (Väyrynen, 1938). Geochemical evidence presented

recently and in this study substantiates this view. Hanski & Smolkin (1989) and Hanski *et al.* (1990) showed with the aid of major, trace element and isotope data that ferropicrite lavas and Ni-bearing gabbro–wehrlite intrusions are cogenetic. The isotopic compositions of Pb in sulphide ores and ferropicritic rocks form a linear array in the $^{208}Pb/^{204}Pb$–$^{206}Pb/^{204}Pb$ space, implying a common origin (Pushkarev *et al.*, 1988; Hanski *et al.*, 1990). The PGE concentrations of many cumulate rocks from the differentiated flows and intrusions overlap with those observed in the massive flows. Furthermore, the concentrations of chalcophile elements and precious metals of the gabbroic cumulates of several intrusions and layered flows (Figs 3 and 4) are low or even below the detection limit of the analytical method. This observation suggests that segregation and accumulation of sulphides were important processes during the formation of these rocks. The normalized concentrations of Ni, Cu and PGE in the disseminated sulphide ores are parallel to those of the ferropicrite flows (Fig. 7). This indicates that the sulphide liquid was derived from an ultramafic magma and hence links the formation of the disseminated sulphides to the evolution of the ferropicritic magma.

The formation of the massive and breccia ores is a point of debate. In their review on the Pechenga ore field, Zak *et al.* (1982) suggested that the massive, breccia and vein ores were produced during regional metamorphism. However, the gradual increase in the amount of sulphide from disseminated ore to massive ore in many intrusions (Figs 3 and 4) and the good correlation among all ore components (Fig. 5) favour the pooling of the sulphide liquids at the base of the intrusion during the magmatic stage. Nevertheless, the PGE patterns of the massive and breccia ores appear to define two types. One, as described above, has relatively low Pt/Ir ratios (<25) and a flat PGE distribution pattern that parallels the pattern of the parental magma (filled symbols in Fig. 7b). The other type (open symbols in Fig. 7b) has much lower Ir, Os and Ru, but higher Pt and Pd concentrations, resulting in high Pt/Ir ratios (>25). These two types are not randomly distributed. Samples from the Pilgujärvi and Kaula intrusions have low Pt/Ir ratios whereas those from the Kotselvaara, Kammikivi and Ortoaivi sills belong to the type having low Ir, Os and Ru concentrations and high Pt/Ir ratios.

The Os-isotopic composition of the ore samples also distinguishes these two types (Walker *et al.*, 1997): samples from the Pilgujärvi intrusion have γ_{Os} values of <50, whereas those of the Kammikivi, Ortoaivi and Kotselvaara sills have significantly higher γ_{Os} values, generally >100 [γ_{Os} defines the percent deviation of the $^{187}Os/^{188}Os$ ratio of a sample from that of the chondritic reservoir (Shirey & Walker, 1998)]. The large variation of the Os isotopic composition in the ferropicritic rocks has been explained by assimilation of variable amounts of radiogenic pelitic sediments (γ_{Os} >300) during the emplacement of the intrusions (Walker *et al.*, 1997).

One possible explanation for the differences in the PGE patterns is that the sulphide liquids formed in different parental magmas. As ultramafic magmas fractionate (without sulphide liquid) they become more Pd and Pt rich but depleted in Ir, Os and Ru. Thus, the pattern of the group of sulphides with high Pt/Ir and γ_{Os} values could be explained if they were derived from a parental magma more fractionated than that forming the sulphides with relatively low Pt/Ir and γ_{Os} values. The high γ_{Os} values in sulphide ores of the Kammikivi sill, compared with the Pilgujärvi samples, can be explained by its higher susceptibility to the effects of contamination as a result of the lower Os content of its parental magma.

Although variations in the composition of the parental magma certainly have occurred, some observations indicate the involvement of an additional process, namely fractional crystallization of the sulphide liquid during its accumulation at the bottom of the host intrusion. In some intrusions the Os-isotopic composition of the barren cumulates is different from that of the sulphide ores beneath. For example, in the drill hole Pet1 sampling the Kammikivi sill, olivine cumulates and chromite separates have γ_{Os} values of ~20, but the sulphide-rich rocks beneath have values of ~250 (Walker *et al.*, 1997). Furthermore, sulphide-poor samples in the same drill hole have low Pt/Ir ratios (<25) similar to those of the massive ferropicrite flows. But in the sulphide-rich rocks beneath, the Pt/Ir ratio is higher and tends to increase with stratigraphic depth from 28·9 to 79·4 (Table 2). These observations indicate that high Pt/Ir ratios and γ_{Os} values are specific features of the sulphide-rich samples and are not directly related to the parental silicate magma. Another interesting observation is that there is no good correlation among many of the chalcophile and siderophile metals in sulphide-rich rocks (>10 wt % S). For example, the Cu content in these samples varies by a factor of 30, but Ni contents are fairly constant ranging only from 2 to 7 wt % (Fig. 5a). Similarly, Pd and Pt concentrations in sulphide-rich rocks vary by more than one order of magnitude and they are correlated, whereas Rh, Ir, Ru and Os concentrations vary less and are not well correlated with Pd or Pt (Fig. 5). Thus, in the ore samples, concentrations of Ni, Ir, Os, Ru and Rh are buffered or even decrease as the Cu, Pd and Pt concentrations increase (Fig. 9). This behaviour of the PGE, Cu and Ni has also been observed in massive ores from the Sudbury and Noril'sk deposits, and has been explained by fractional crystallization of the sulphide liquid (Naldrett *et al.*, 1994*a*, 1994*b*). These studies found that Cu, Pd and Pt become concentrated in the residual sulphide liquid, and Ni, Ir and Rh in the monosulphide solid solution as the parental sulphide liquids crystallizes.

These observations have been confirmed by experimental studies (e.g. Barnes *et al.*, 1997; Ebel & Naldrett, 1997) where the partition coefficients between monosulphide solid solution (Mss) and sulphide liquid ($D_{mss/sul}$) for Pd, Pt and Cu are <0·4, whereas those of Ir, Rh and Ni tend to be >1. These results are broadly consistent with the PGE patterns observed in Fig. 7b, if one assumes that the ore type with flat patterns represents the parental sulphide liquid (filled symbols), whereas those patterns showing relative deletion of Ir, Os and Ru and enrichment of Pd and Pt represent the residual sulphide liquid (open symbols).

Quantitative description of the formation and crystallization of the sulphide liquid

The observations described above are consistent with a simple model that assumes that the parental ferropicrite magma became sulphur saturated during its emplacement. This triggered sulphide immiscibility and the segregation and accumulation of a sulphide liquid at the bottom of the intrusions. Upon cooling, this parental sulphide liquid crystallized forming an Fe-rich monosulphide solid solution and a Cu–Pd–Pt-rich sulphide liquid. The composition of the parental sulphide liquid and its crystallization can be modelled by using the sulphide–silicate partition coefficients estimated in this study. The partition coefficient between monosulphide solution and sulphide liquid have been determined by Barnes *et al.* (1997) and Ebel & Naldrett (1997). Those workers have shown that the partition coefficients in the sulphide system strongly depend on the composition (S content), temperature and fO_2/fS_2 of the sulphide liquid. As these factors are not known for the Pechenga sulphide liquids, average values have been chosen for the model calculations. The parameters and model calculations are given in Table 5 and the results are shown in Fig. 9, where the Ir concentrations in the sulphide liquid are plotted against the Pt/Ir and Cu/Ir ratios. For example, using the samples with the highest S contents (>10%) and normalizing their PGE contents to 100% sulphide, it is calculated that the Ir content of the sulphide liquids ranged from 2 to 520 ng/g (Fig. 9).

The model calculations assume that sulphide saturation occurred in the least PGE-depleted ferropicritic magma and the metal concentration in the parental sulphide liquid has been calculated by applying the equation of Campbell & Naldrett (1979):

$$C^0_{sul} = \frac{D_{sul/sil}(R + 1)C^0_{sil}}{R + D_{sul/sil}} \quad (3)$$

where $D_{sul/sil}$ represents the sulphide–silicate partition coefficient, R the silicate/sulphide mass ratio, C^0_{sul} the element concentration in the parental sulphide liquid and C^0_{sil} the element concentration in the parental silicate liquid.

The model calculation shows that the parental sulphide liquid should originally have had Pt/Ir and Cu/Ir ratios that are similar to or slightly lower than those of the parental silicate magma (Table 5; Fig. 9). This inference is the result of the low R-factors (<1000) that are necessary to explain the low Ir (PGE) tenor in the sulphide samples. Such low R-factors are typical for sulphides derived from ultramafic magmas, such as the deposits of Kambalda in Australia (Duke, 1990). Only a few samples with about 100 ng/g Ir (recalculated to 100% sulphide) straddle the trend defined by the calculated compositions of parental sulphide liquids in equilibrium with the least PGE depleted ferropicrites (Fig. 9). Some samples appear to follow a parallel trend with lower Ir concentrations and higher, but relatively constant Pt/Ir (10–30) and Cu/Ir ratios. These sulphide liquids are probably derived from silicate melts that had a lower Ir concentration and higher Pt/Ir and Cu/Ir ratios than the presumed parental ferropicrite composition as a result of previous events of sulphide segregation.

However, most of the sulphide samples follow a trend of increasing Pt/Ir and Cu/Ir ratios as the Ir concentrations decrease from ~100 to 10 ng/g. This trend can be explained by 40–50% of fractional crystallization of monosulphide solid solution (Table 5; Fig. 9). Similar calculations can be made using Pd and Rh, assuming $D_{mss/sul}$ values of 0·2 and >1·0, respectively. These values are within the range of values determined experimentally. For Os and Ru there are no experimental data available. A close look at Fig. 7b indicates that the residual sulphide liquid is more depleted in these metals relative to Ir. This implies that the $D_{mss/sul}$ values of these metals are greater than that of Ir.

In principle, the $D_{mss/sul}$ of the different metals can be estimated from the dataset by applying the same reasoning and technique as used before to determine the sulphide–silicate partition coefficients. However, as discussed above, the compositions of the parental sulphide liquids were not uniform, because the liquid segregated from silicate melts with variable initial PGE concentrations and because the sulphide–silicate mass ratio probably was different in each intrusion. In addition, many of the ore samples probably do not represent pure liquid compositions but are cumulates consisting of variable proportions of Mss and residual sulphide liquid.

Nevertheless, the calculations confirm our suggestion that the two ore types defined by the different PGE patterns in Fig. 7b are related by the crystallization of monosulphide solid solution from a number of parental sulphide liquids. The Cu–Pt–Pd-rich but Ir-, Os- and Ru-poor samples reflect the residual sulphide liquid. Unfortunately, the present dataset does not include many

samples representing the Os-, Ir- and Ru-rich monosulphide solid solution. Sulphides having Ir contents of 35–520 ng/g Ir and low Pt/Ir (<6) and Cu/Ir ratios (<0·1) appear to be the closest representatives (Fig. 9).

The model explains additional features, such as the occurrence of chalcopyrite-rich shale-hosted veins and the extremely high γ_{Os} values (>100) of some of the ores (Walker *et al.*, 1997). After the crystallization of Mss, the residual sulphide liquid is highly mobile and reactive as a result of its low viscosity and strong wetting properties (Ebel & Naldrett, 1997). Hence, during cooling and compaction the residual liquid can be easily squeezed out from the sulphide pool at the bottom of an intrusion into the underlying sediments, forming sulphide veins and impregnations. These features also allow the liquid to react with or even partly assimilate sediments. Assimilation of Re and radiogenic Os from the sediments by the sulphide liquid would explain the highly radiogenic nature of Os in sulphides from the Pet1 drill core compared with that of the overlying silicate cumulates (Walker *et al.*, 1997).

Cause of sulphide saturation: assimilation of S-rich sediments

One question that has not been addressed so far is the cause of sulphide saturation and the source of sulphur in the ores. The high PGE concentrations in several ferropicrite lavas may indicate that they could have reached the surface S undersaturated. But most flows are depleted in PGE and were S saturated as discussed above. Crustal contamination has been invoked as a process triggering sulphide saturation in mafic and ultramafic magmas (Irvine, 1975). The existence of breccias and inclusions of sedimentary country rocks in some Ni-bearing intrusions suggests that the assimilation of sulphur-rich sediments during the intrusion of the ferropicrite magma caused sulphide saturation. However, large amounts of assimilation of continental crust by the ferropicritic magma is unlikely because of the high ε_{Nd} value of +1·6 of ferropicritic volcanic rocks and cumulates from the Pilgujärvi intrusion (Hanski *et al.*, 1990). Nevertheless, little variation of the ε_{Nd} has to be expected, because the Nd concentration in the ferropicrite magma was relatively high and the sediments did not have very radiogenic Nd isotopic compositions [an S-rich phyllite from the Kotselvaara quarry yielded an initial ε_{Nd} value of −0·3 (H. Huhma, unpublished data, 1999)]. Therefore contamination with sedimentary material is not easily recognized with the Nd isotopic composition of the ferropicrites.

Pushkarev *et al.* (1988) have published Pb-isotope data of ore-bearing intrusions and related Ni–Cu ores, ferropicritic volcanic rocks as well as iron sulphides from phyllites. These data, and additional analyses by Hanski *et al.* (1990), show that on a $^{208}Pb/^{204}Pb$ vs $^{206}Pb/^{204}Pb$ diagram, the ferropicritic volcanic rocks and the cumulates of gabbro–wehrlite intrusions plot along a line passing through the field of Ni–Cu sulphides and do not provide evidence for large differences between ore-bearing and barren ferropicrites. This again precludes the assimilation of large amounts (>10%) of sediments by Ni-bearing intrusions. However, careful calculations of the slopes of the Pb-isotope variations reveal that the Pilgujärvi intrusion has a slightly lower Th/U ratio (Th/U = 3·2) than the ferropicrite volcanic rocks (Th/U = 3·9). This decrease in the Th/U ratio can be explained by bulk contamination of a ferropicrite magma with 2–6% of sediments.

The isotopic composition of Os determined by Walker *et al.* (1997) provides the most convincing evidence for crustal contamination. The ferropicritic lavas and intrusion display a large γ_{Os} range from ~6 to >200 and that of the sediments can be even as high as 600. As discussed above, the most radiogenic signature in some sulphide ores is probably the result of assimilation of sediment by the sulphide liquid. However, even sulphide-poor or barren rocks and mineral separates have γ_{Os} values of up to 80. Walker *et al.* (1997) explained this variation by assimilation of up to 10% of sediments by the ferropicritic magma.

Grinenko *et al.* (1967) and Pushkarev *et al.* (1988) published sulphur isotope determinations on many Ni–Cu sulphide deposits from the Kola Peninsula. They did not observe differences in the isotopic composition of S between disseminated and massive and breccia ores from Pechenga and therefore inferred a common and predominantly mantle source of sulphur for the main ore types.

Grinenko & Smolkin (1991) provided S-isotope data for sediments and sulphide-poor ferropicrite lavas. The $\delta^{34}S$ values for sediments range from −7 to +12‰ but the data display two abundance maxima, the first in the interval −4 to +2‰, the second between +4 and +6‰, suggesting two different sulphur sources. The ferropicrite lavas and gabbro–wehrlite intrusions display variable S-isotope compositions with $\delta^{34}S$ ranging from −3 to 8‰ (Grinenko & Smolkin, 1991; Melezhik *et al.*, 1994*a*) but consistently the margins of the layered bodies show higher $\delta^{34}S$ than their interiors. Grinenko & Smolkin (1991) suggested that local assimilation of country-rock sulphur during emplacement of the flow caused the high $\delta^{34}S$ at the margin.

Similarly, Melezhik *et al.* (1994*a*) emphasized the large variation of $\delta^{34}S$ in the ferropicritic rocks. They suggested that the S isotopic composition of the parental magmas was initially mantle-like ($\delta^{34}S$ = −0·5–1·5‰) but has been modified by sediment assimilation during the magma emplacement. Those workers also proposed that the average S contents of the ferropicritic flows and

intrusions are too high to be of pure mantle origin. They calculated that ~25–65% of the sulphur is derived from the sediments.

In summary, sulphur and radiogenic isotope data are consistent with the hypotheses that during eruption and intrusion into the productive pile the ferropicrite magma locally assimilated sediments. However, trace element and isotope data constrain the amount of contamination to <10%. Unfortunately, the S content and the S solubility of the ferropicrite melt are not well constrained. It is, therefore, not apparent whether this amount of assimilation was sufficient to trigger sulphide saturation in the ferropicrite melt.

CONCLUSIONS

Very important Ni–Cu sulphide resources are found in the intracontinental environment and are associated with ultramafic volcanic rocks, such as komatiites, and with basalt provinces derived from mantle plumes. The deposits of the Pechenga Complex are also associated with ultramafic ferropicritic volcanic and intrusive bodies that are part of a thick volcanic–sedimentary sequence.

Trace element and isotope data have shown that gabbro–wehrlite intrusions hosting the mineralization and ferropicritic lava flows are comagmatic. Intrusive and volcanic rocks were derived from a parental magma that had MgO contents of 15–19 wt % and was unusually rich in FeO, averaging 15–16 wt % (e.g. Hanski, 1992). These features have been acquired during the partial melting process and assert the unusual mantle composition from which the ferropicrites have been derived.

The radiogenic initial Os isotopic composition (γ_{Os} ~6) obtained for the ferropicritic parental magma is also unusual because the Pechenga ferropicrites are the oldest rocks showing evidence for the presence of a mantle source with a long-term Re enrichment (Walker *et al.*, 1997). However, the PGE concentrations do not indicate unusually high abundances in the source region, as the maximum concentration of ~7 ng/g Pt and Pd, 2 ng/g Ir, Os and Ru, and low Pd/Ir ratios (~10) are typical features of ultramafic magmas.

Segregation and accumulation of sulphide liquids mainly controlled the distribution of the PGE in the lava flows and intrusive bodies. In several differentiated flows and layered intrusion the PGE concentrations together with S and Cu contents systematically increase towards the base of the magma bodies. The highest concentrations of chalcophile and siderophile elements occur in massive sulphides at the contact of intrusion and host rock, reaching ~4 wt % Cu, 7 wt % Ni, 1 μg/g Pt and Pd and <90 ng/g Ir, Os, Rh or Ru. In volcanic rocks closely representing the liquid composition of the ferropicrite melt all PGE correlate well with each other and behave compatibly. This PGE distribution can be described by the fractional segregation of a sulphide liquid. This model predicts that the relative sulphide–silicate partition coefficients vary by a factor of 1·9 and decrease in the sequence of Ir, Rh, Os, Ru, Pt, Pd. Assuming that the partition coefficients are of the order of 45 000–85 700 (Fig. 6) only very small amounts of sulphide, which imply large *R*-factors of 10^4–10^5, are necessary to describe the PGE variation in the ferropicritic flows. The significantly different sulphide–silicate partition coefficients for Pd and Ir and the high *R*-factor cause the fractionation of Pt and Pd from Ir as sulphides are segregating, thus Pt/Ir or Pd/Ir ratios increase with decreasing Ir concentrations (Fig. 9).

Sulphide immiscibility was probably triggered by the assimilation of S-rich sediments hosting the ore-bearing intrusions. The sulphide liquids segregated and pooled at the base of the intrusions. Then, during fractional crystallization of Mss, massive sulphide ores formed at the interface of intrusion and underlying sediments. In some cases the residual sulphide liquid has been squeezed out and filled open faults and cavities in the country rock.

The low PGE tenor in massive sulphides implies low *R*-factors of <1000. As a consequence, the parental sulphide liquids must have had PGE ratios, such as Pt/Ir, that were similar to that of the silicate liquid from which they were derived. However, many of the sulphides have higher Pt/Ir ratios. This observation can partly be explained if the parental sulphide liquid equilibrated with ferropicritic melts of varying composition as a result of the fractionation of silicates, oxides or sulphide liquids. In addition, ratios such Pt/Ir, Pd/Ir, Pt/Os or Pt/Ru have been increased during the fractionation of the parental sulphide liquid as Mss crystallized. During this process Pd and Pt become enriched whereas Ir, Os and Ru become depleted in the residual sulphide liquid. Its chemo-physical properties suggest that the sulphide liquid is highly mobile and is able to partly assimilate sedimentary country rocks.

ACKNOWLEDGEMENTS

We thank M. Assif for his assistance during the analytical determination of the PGE. The suggestions of M. Sharma and A. W. Hofmann, and the reviews by R. Wendlandt, R. Frey and J. Kazuba improved the manuscript. We thank I. Bambach and G. Feyerherd for helping us to prepare the figures.

REFERENCES

Abzalov, M. Z. & Both, R. A. (1997). The Pechenga Ni–Cu deposits, Russia: data on PGE and Au distribution and sulphur isotope compositions. *Mineralogy and Petrology* **61**, 119–143.

Asif, M. & Parry, S. J. (1989). Elimination of reagent blank problems in the fire assay preconcentration of the platinum-group-elements and Au with a sulfide bead weighting less than one gram. *Analyst* **114**, 1057–1059.

Asif, M. & Parry, S. J. (1990). Nickel sulfide assay for the collection of the platinum-group-elements and Au from chromitites using reduced bead size. *Mineralogy and Petrology* **42**, 321–326.

Balashov, Y. A. (1996). Paleoproterozoic geochronology of the Pechenga–Varzuga structure, Kola Peninsula. *Petrology* **4**, 1–22.

Barnes, S.-J., Makovicky, E., Makovicky, M., Rose-Hansen, J. & Karup-Moller, S. (1997). Partition coefficients for Ni, Cu, Pd, Pt, Rh, and Ir between monosulphide solid solution and sulfide liquid and the formation of compositionally zoned Ni–Cu sulfide bodies by fractional crystallisation. *Canadian Journal of Earth Sciences* **34**, 366–374.

Bezmen, N. I., Asif, M., Brügmann, G. E., Romanenko, I. M. & Naldrett, A. J. (1994). Distribution of Pd, Rh, Ru, Ir, Os and Au between sulfide and silicate melts. *Geochimica et Cosmochimica Acta* **58**, 1251–1260.

Brügmann, G. E., Arndt, N. T., Hofmann, A. W. & Tobschall, H.-J. (1987). Precious metal abundances in komatiite suites from Alexo, Ontario, and Gorgona Island, Colombia. *Geochimica et Cosmochimica Acta* **51**, 2159–2169.

Brügmann, G. E., Naldrett, A. J., Asif, M., Lightfoot, P. C., Gorbachev, N. S. & Federenko, V. A. (1993). Siderophile and chalcophile metals as tracers of the evolution of the Siberian Trap in the Noril'sk region, Russia. *Geochimica et Cosmochimica Acta* **57**, 2001–2018.

Campbell, I. A. & Naldrett, A. J. (1979). The influence of silicate:sulfide ratios on the geochemistry of magmatic sulfides. *Economic Geology* **74**, 1503–1506.

Distler, V. V., Filimonova, A. A., Grokhovskaya, T. L. & Laputina, I. P. (1990). Platinum-group elements in the copper–nickel ores of the Pechenga ore field. *International Geological Review* **32**, 83.

Duke, J. M. (1990). Mineral deposits models: nickel sulfide deposits of the Kambalda type. *Canadian Mineralogist* **28**, 379–388.

Ebel, D. S. & Naldrett, A. J. (1997). Crystallisation of sulphide liquids and the interpretation of ore composition. *Canadian Journal of Earth Sciences* **34**, 352–365.

Gorbunov, G. I. (1968). *Geology and Genesis of the Pechenga Ni–Cu Sulfide Deposits*. Moscow: Nedra, 352 pp. (in Russian).

Gorbunov, G. I., Yakovlev, Yu. N., Goncharov, Yu. V., Gorelov, V. A. & Telnov, V. A. (1985*a*). The nickel areas of the Kola Peninsula. In: Papunen, H. & Gorbunov, G. I. (eds) *Nickel–Copper Deposits of the Baltic Shield and Scandinavian Caledonides. Geological Survey of Finland, Bulletin* **333**, 41–109.

Gorbunov, G. I., Zagorodnyi, V. G. & Robonen, W. I. (1985*b*). Main features of the geological history of the Baltic Shield and the epochs of ore formation. In: Papunen, H. & Gorbunov, G. I. (eds) *Nickel–Copper Deposits of the Baltic Shield and Scandinavian Caledonides. Geological Survey of Finland, Bulletin* **333**, 17–41.

Grinenko, L. N. & Smolkin, V. F. (1991). Isotopic composition and content of sulfur in ferropicrites and gabbro–wehrlite intrusions of the Pechenga Zone. *Geokhimiya* **9**, 1250–1261 (in Russian)

Grinenko, L. N., Grinenko, V. A. & Lyakhnitskaya, I. V. (1967). Sulfur isotope composition of sulfides from copper–nickel deposits in the Kola Peninsula. *Geologiya Rudnykh Mestorozhdenii* **4**, 3–17 (in Russian).

Hanski, E. (1992). *Petrology of the Pechenga Ferropicrites and Cogenetic Ni-bearing Wehrlite Intrusions, Kola Peninsula, Russia. Geological Survey of Finland, Bulletin* **367**, 192 pp.

Hanski, E. & Smolkin, V. F. (1989). Pechenga ferropicrites and other early Proterozoic picrites in the eastern part of the Baltic Shield. *Precambrian Research* **45**, 63–82.

Hanski, E. & Smolkin, V. F. (1991). Spinifex-textured ferropicritic flows in the Pechenga area, Kola Peninsula. *GAC–MAG–SEG Joint Annual Meeting, Program with Abstracts* **16**, A51.

Hanski, E. & Smolkin, V. F. (1995). Iron- and LREE-enriched mantle source for early Proterozoic intraplate magmatism as exemplified by the Pechenga ferropicrites, Kola Peninsula, Russia. *Lithos* **34**, 107–125.

Hanski, E., Huhma, H., Smolkin, V. F. & Vaasjoki, M. (1990). The age of the ferropicritic volcanics and comagmatic Ni-bearing intrusions at Pechenga, Kola Peninsula, USSR. *Bulletin of the Geological Society of Finland* **62**, 123–133.

Irvine, T. N. (1975). Crystallization sequences of the Muskox intrusion and other layered intrusions—II. Origin of chromite layers and similar deposits of other magmatic ores. *Geochimica et Cosmochimica Acta* **39**, 991–1020.

Lesher, C. M. (1989). Komatiite-associated nickel sulfide deposits. In: Whitney, J. A. & Naldrett, A. J. (eds) *Ore Deposition Associated with Magmas. Reviews in Economic Geology* **4**, 45–103.

Melezhik, V. A. & Sturt, B. A. (1998*a*). The early Proterozoic Pechenga–Varzuga Belt: a case of back-arc spreading by Evgenii V. Sharkov and Valery Smolkin (1997) *Precambrian Research* **82**, 133–151: Comments. *Precambrian Research* **92**, 215–218.

Melezhik, V. A. & Sturt, B. A. (1998*b*). The Paleoproterozoic (2·5–1·7 Ga) Midcontinent rift system of the northeastern Fennoscandian Shield versus the early Proterozoic Pechenga–Varzuga belt: a case of back-arc spreading. Discussion. *Canadian Journal of Earth Sciences* **35**, 720–725.

Melezhik, V. A., Hudson-Edwards, K. A., Green, A. H. & Grinenko, L. N. (1994*a*). Pechenga area, Russia—Part 2: Nickel–copper deposits and related rocks. *Institution of Mining and Metallurgy, Transactions, Section B: Applied Earth Sciences* **103**, 146–161.

Melezhik, V. A., Hudson-Edwards, K. A., Skuf'in, P. K., Green, A. H. & Nilsson, L.-P. (1994*b*). Pechenga area, Russia—Part 1: geological setting and comparison with Pasvik, Norway. *Institution of Mining and Metallurgy Transactions, Section B: Applied Earth Sciences* **103**, 129–145.

Melezhik, V. A., Sturt, B. A., Mokrousov, V. A., Ramsay, D. M., Nilsson, L. P. & Balashov, Y. A. (1995). The Early Proterozoic Pasvik–Pechenga Greenstone Belt, 1:100,000 geological map, stratigraphic correlation and revision of stratigraphic nomenclature. In: Roberts, D. & Nordgulen, Ø. (eds) *Geology of the Eastern Finnmark–Western Kola Region. Norges Geologiske Undersøkelse, Special Publication* **7**, 81–92.

Mitrofanov, F. P., Balashov, Yu. A. & Balagansky, V. V. (1991). New geochronological data on lower Precambrian complexes of the Kola Peninsula. In: Mitrofanov, F. P. & Balagansky, V. V. (eds) *Correlation of Lower Precambrian Formations of the Karelian–Kola Region, USSR and Finland*. Apatity: Geological Institute, Kola Science Centre of the USSR Academy of Sciences, pp. 12–16.

Naldrett, A. J., Asif, M., Gorbachev, N. S., Kunilov, V. I., Stekhin, A. I., Fedorenko, V. A. & Lightfoot, P. C. (1994*a*). The composition of the Ni–Cu ores of the Noril'sk region. *Ontario Geological Survey Special Publication* **5**, 357–372.

Naldrett, A. J., Pesseran, A., Asif, M. & Li, C. (1994*b*). Compositional variations in the Sudbury ores and predictions of the proximity of footwall copper–PGE ore bodies. *Ontario Geological Survey Special Publication* **5**, 133–146.

Papunen, H. & Gorbunov, G. I. (eds) (1985). *Nickel–Copper Deposits of the Baltic Shield and Scandinavian Caledonides. Geological Survey of Finland, Bulletin* **333**, 394 pp.

Peach, C. L., Mathez, E. A., Keays, R. R. & Reeves, S. J. (1990). Experimentally determined sulfide melt–silicate melt partition coefficients for iridium and palladium. *Geochemical Geology* **117**, 361–377.

Puchtel, I. S., Arndt, N. T., Hofmann, A. W., Haase, K. M., Kröner, A., Kulikov, V. S., Kulikova, V. V., Garbe-Schönberg, C.-D. & Nemchin, A. A. (1998). Petrology of mafic lavas within the Onega

Plateau, central Karelia: evidence for 2·0 Ga plume related continental crustal growth in the Baltic Shield. *Contributions to Mineralogy and Petrology* **130**, 134–153.

Pushkarev, Yu. D., Ryungenen, G. I., Smolkin, V. F. & Shurkina, L. K. (1988). The Pb isotope geochemistry and generation of nickel-bearing basic–ultrabasic rocks in the Kola Peninsula. In: Shukolyukov, Yu. A. (ed.) *Isotope Geology and Processes of Ore Formation*. Leningrad: Nauka, pp. 150–166 (in Russian).

Sharkov, E. V. & Smolkin, V. F. (1989). High titanian ferropicrites—specific magmatic formations in the transition period from early to late Proterozoic. *Doklady Akademii Nauk SSSR* **309**, 164–168 (in Russian).

Sharkov, E. V. & Smolkin, V. F. (1998). Reply. *Precambrian Research* **92**, 219–221.

Shirey, S. B. & Walker, R. J. (1998). The Re–Os isotope system in cosmochemistry and high-temperature geochemistry. *Annual Review of Earth and Planetary Sciences* **26**, 423–500.

Skuf'in, P. K. & Fedotov, Zh. A. (1989). Picritic pillow lavas in the section of the early Proterozoic volcanics of the Pechenga structure. *Doklady Akademii Nauk SSSR* **306**, 956–962 (in Russian).

Smolkin, V. F. (1977). *Petrology of the Pilgujärvi Ore-bearing Intrusion*. VINITI, No. 2114–77. Apatity: Geological Institute of the Academy of Science of the USSR, 216 pp. (in Russian).

Smolkin, V. F. (1997). The Paleoproterozoic (2·5–1·7 Ga) Mid-continental rift system of the northastern Fennoscandian Shield. *Canadian Journal of Earth Sciences* **34**, 426–443.

Smolkin, V. F. (1998). The origin of the Paleoproterozoic belt (north-eastern Fennoscandian Shield). Reply. *Canadian Journal of Earth Sciences* **35**, 726–733.

Smolkin, V. F., Borisov, A. E. & Marakushev, A. A. (1987). Signs of differentiation and immiscibility of picrito-basaltic liquids at Pechenga. *Doklady Akademii Nauk SSSR* **294**, 669–673 (in Russian).

Smolkin, V. F., Skuf'in, P. K. & Mokrousov, V. A. (1995). Stratigraphic position, geochemistry and genesis of volcanic associations of the Early Proterozoic Pechenga area. *Norges Geologiske Undersøkelse, Special Publication* **7**, 50–75.

Smolkin, V. F., Skuf'in, P. K., Mitrofanov, F. P. & Mokrousov, V. A. (1996). Stratigraphy and volcanism in the early Proterozoic Pechenga structure (Kola Peninsula). *Stratigraphy and Geological Correlation* **4**, 78–94.

Stone, W. E., Crocket, J. H. & Fleet, M. E. (1990). Partitioning of Pd, Ir, Pt and Au between sulfide liquid and basalt melt at 1200°C. *Geochimica et Cosmochimica Acta* **54**, 2341–2344.

Väyrynen, H. (1938). Petrologie des Nickelerzfeldes Kaulatunturi–Kammikivitunturi in Petsamo. *Bulletin de la Commission Géologique de Finlande* **116**, 1–198.

Walker, R. J., Morgan, J. W., Hanski, E. J. & Smolkin, V. F. (1997). Re–Os systematics of Early Proterozoic ferropicrites, Pechenga Complex, northwestern Russia: evidence for ancient ^{187}Os-enriched plumes. *Geochimica et Cosmochimica Acta* **61**, 3145–3160.

Zak, S. I., Makarov, V. N., Kochnev-Pervukhov, V. I., Proskuryakov, V. V., Zaskind, E. S., Batashev, E. V. & Kolesnikov, G. P. (1982). *Geology, Magmatism and Ore Formation in the Pechenga Ore Field*. Leningrad: Nedra, 112 pp. (in Russian).

Zagorodnyi, V. D., Mirskaya, D. D. & Suslova, S. N. (1964). *Geologicheskoe stroenie Pechengskoi osadochno-vulknogennoi serii*. Moscow: Nauka, 208 pp.